

## **PROJECT REPORT**

Sreeja Nag (Summer Intern -  
Jet Propulsion Laboratory, California Institute of Technology)

[sreejanag@gmail.com](mailto:sreejanag@gmail.com)

Advisor : Dr. Paul R. Lundgren

NASA Planetary Geology and Geophysics Undergraduate Research Program

### **INTRODUCTION**

Mars has long been known to share many similarities with Earth. Geologic and evolutionary differences are explained largely by differences in size and orbital distance from the Sun. Perhaps the single most apparent feature of Mars is its crustal dichotomy, as represented by its global topography and crustal thickness variations [Zuber *et al.*, 2000; Zuber, 2001; Neumann *et al.*, 2004]. Graben and pit craters are found over much of Mars and may be closely linked to both the creation of large flood events and the channeling of fluids in its subsurface. Determining the causes of the large numbers of fractures, graben, and pit crater chains on Mars is fundamental toward understanding the structural development of the planet's surface and the interaction of the mantle with the near surface and surface environment. Our objectives are:

- To understand the 3-D structures and processes related to graben and pit crater variability in size and distribution.
- To determine the effects of regional stresses on the development of groups of fracture systems. For example, this would include understanding what controls the parallel variations in graben and pit crater sizes in some areas..

We focused on graben and pit crater chains of the Alba Patera region. (Figure 1)

To constrain models for the mechanics and development of these graben-pit catenae structure, 3-D numerical mechanical analyses has been proposed, of which I shall be using boundary element modeling to help understand both individual, and complex groups of graben and pit chains on Mars. The models will account for the interaction of structures in the graben and pit chains. The numerical modeling will yield surface displacements and stress fields that will be directly compared to the structures at the surface of Mars as seen in MOLA topography, and MOC and THEMIS images.

Graben and pit crater chains or catenae are found extensively on Mars, with fractures and graben in many places extending for hundreds of kilometers. Many of these are associated with plume-related uplift and volcanism of the Tharsis region [Tanaka, 1990; Wilson and Head, 2002]. Whether graben and pit crater chains are associated with regional tectonic extension or long radial dikes is not entirely clear. The mechanism for pit crater formation is a matter of debate, with more than one process possible for different sets of pit craters. By their very nature, pit craters have

been considered to form either as the direct result of shallow crustal fluids or volatiles, or if from a magmatic or tectonic mechanism, then above structures that are likely conduits for fluid flow in the near surface [Wyrick *et al.*, 2004]. The main candidates proposed include:

- 1) Karst processes
- 2) Opening mode cracks
- 3) Dike intrusion
- 4) Dilation above a normal fault

## **BASIC APPROACH**

We applied 3-D numerical software that take into account the full 3-D displacements and stress fields generated by fracture systems under a range of crustal conditions and that account for mechanical interaction. Our primary observational constraint for these models for Mars was the surface topography, which requires assembling MOLA profiles. Our approach was to apply a 3-D boundary element code [*Poly3D*; Thomas, 1993; Okubo and Martel, 1998] to test which types of structures (i.e. normal faults, tensile cracks or dikes) beneath graben systems best fit the surface topography by matching the elastic solution in half space (details later). An important contribution of these 3D numerical models is the ability to test complex source structures. Observations of Mars suggest more than one type of mechanism is present (e.g., simple graben *and* radial dikes). We tested different source models and stress conditions by comparing the numerical solutions for fault slip and surface displacement with surface observations.

Initially for Mars, we considered stress conditions that favor the development of pit craters and grabens rather than trying to model the micromechanics of their actual development. We used observations on pit crater distribution and size *a posteriori* to evaluate subsurface models. The primary constraints on model parameters (e.g. fracture location, geometry, sense of slip) comprised topography and imagery observations. We explored a range of stress drops on faults and driving pressures on dikes to evaluate model sensitivity to those parameters and developed forward models to understand the main differences between the candidate source types (i.e., tensile fractures, normal faults at depth, and dikes). Depending on the data quality and surface structure complexity, inverse models could be developed, but this is more time consuming than developing simpler forward models, and may be beyond the scope of this project.

## **BACKGROUND**

Similar approaches have been followed, implemented on a variety of Martian terrains and published over the last decade. The data and forward models have mainly been 2D, hence more literature is available for approximately E-W trending features because the MOLA profiles from the MGS are the primary source of data. Since the MGS is in polar orbit, the MOLA profiles intersect EW trending features almost

orthogonally, making the data more reliable. *Schultz et al (2004)* investigated the Tharsis radial grabens within Memnonia region of Mars by fitting topography over a simple graben with a dike intrusion and forcing multiple such events (Figure 2a). They also introduced an “hourglass” model since it agreed with data that showed fault offsets decreasing toward fault tips (2000) as shown in Figure 2b. Direct surface topography can be linked to the modes of formation via observation too. *Okubo and Schultz (2005)*, at SE Alba Patera and Valles Marines, demonstrated that Characteristic concave-up surface topography is usually produced by two normal faults, concave-down produced by a dike intrusion and a mixed mode also possible (Figure 2c). Asymmetry can be due to single normal faults, antithetic faulting, unequal fault dips and offset magnitudes on either side of the graben. An example of NS trending grabens is the analysis by *Polit et al (2005)* of Alba Patera where the region was divided into two regions of different faulting depths due to different depth restrictions. A 3D investigation of the Valles Marines grabens was done by *Schultz and Lin (2001)* using standard geodetic inversion of fault-related topography. Two profiles were concentrated upon, boundary element method was used to understand displacement dependency on fault parameters and the trench floor was used as the datum plane to finally sketch a strength envelope for the region. (Figure 2d)

## **DATA**

MOC and THEMIS have made it possible to incorporate structural analysis of fault systems to evaluate their potential influence on permeability in the martian crust. Quantifying the extent and degree of fault network connectivity with provide key constraints for hydrological models. We used THEMIS images, available at the online image repository to select a potential target site to begin modeling relatively simple 3D grabens. The approximate mural is shown in Figure 3a. The THEMIS instrument (Thermal Emission Imaging System) is aboard the Mars Odyssey Spacecraft. It produces images of resolution 18m/pixel (visual images) and 100m/pixel (IR images). ‘Thermoclinometry’ is a technique used to extract the quantitative component of THEMIS and MOC images by using frequency band analysis to separate albedo and thermal inertia effects from topographic component [*Kirk et al, 2003; Soderblom et al, 2002; Gaddis et al, 2005*]. Atmospheric effects are removed to derive DEM. The Mars Orbital Camera narrow angle image for the same area is also shown (Figure 3b, 3c). The MOC is aboard the Mars Global Surveyor. It takes photographs of resolution 1.5-12m/pixel (Narrow angle), 240 m/pixel (Wide angle) and 7.5 km/pixel (daily global imaging). Unfortunately, HiRise data is not available for the selected region, due to the high resolution, the data coverage of Mars is quite limited. The selected region spans 21.5 to 24 degrees latitude and 265.6 to 288 degrees longitude.

The Mars Orbiter Laser Altimeter aboard the Mars Global Surveyor provided 143 MOLA profiles passing through the selected region and 75629 shots in total. It gives range measurements along profile every ~300 m along MGS ground track. The resolution on MOLA groundtrack is 300 m with footprint of each measurement being 168m. Vertical ranging errors are between 0.23m to 10m (for slopes 1-30° respectively).

The MOLA profiles are available as Precision experiment data records (PEDRs) via NASA's Planetary Data System. The data is made usable by converting it to .TAB files using a *pedr2tab* executable, having specified the region of interest to extract the 20 shot MOLA frames within. Crossover corrections are implemented and the height data along long-lat are extracted from the TAB files using Matlab. The output txt file is used in GMT and the blockmean decimation routine implemented. Finally, the surface routine (tension parameter T=0.5, convergence limit C=1) is used to make the 2D gridfile with x-y resolution of 200 pixels/degree (~60km/grid spacing). The surface routine uses continuous spline in tension method of interpolating curved surfaces and has a curvature of 70935.9. The spatial density of observations varies inversely with pixel size, RMS Error is 0.0403891 and the total no. of iterations is 1549 in 6 parts. *Grdgradient* is used to apply artificial illumination (Min artificial intensity used = -36512.9, Max artificial intensity used = 41760.4) and *pswiggle* shows the position of some MOLA profiles in the 2D interpolated figure. The entire process of data extraction is shown in the form of a flowchart (Figure 4). To check the interpolated quality of the data, the MOLA profile ap201071.TAB was removed from the data, the rest of the profiles to interpolate the grid, GMT routine *grdtrack* used to extract the topography along the removed profile from the grid and compared with the original. The figure (Figure 5) shows a good match, hence the interpolated grid can be used for the purpose of modeling. GMT routine *grd2xyz* converts the grid into a Matlab readable format (Figure 3d, 3e), where from profiles can be extracted.

The main reason for choosing this region was the presence of a graben whose depth increases, almost linearly, in the along strike direction. The shallowest part pinches out as the end of the graben with a slight offset before ending. The deeper part almost resembles a hole after which the depth of the graben abruptly rises, and the width abruptly narrows in the form of a pit crater chain i.e. along strike features from west to east is a deepening graben, followed by a very deep crater followed by a pit crater chain. If 2D profiles were taken across the graben and analysed, it should yield similar results to previous works. It is the 3D structure of the graben that is interesting and a 3D analysis, like the one we are using, may yield informative results. It must be noted however, that grabens may be deeper than they seem due to sediments in wedges.

The MOLA profiles (129 in number) were windowed to keep only the region of interest, i.e. the graben system, constrained within two parallel lines:  $\text{lat} = 0.7143 \cdot \text{long} - 168.1429$  and  $\text{lat} = 0.8333 \cdot \text{long} - 199.3333$ . The sliced profiles are shown in Figure 6. It can be seen that there is a gap in data/profiles around the region of maximum depth. Since the grid size is less than this gap between successive MOLA profiles (at times), interpolation may cause artifacts to form as shown in the profile extracted from the gridded DEM (Figure 7b). The sudden rise in topography within the deepest data points seems to be an interpolation artifact. The DEM can be used for a 3D view of any area and to decide the course of modeling to use, however for detailed fitting, depth points considered for along graben profiles rather than fitting lines through the graben strike direction. Similarly, MOLA profiles considered for cross-graben profiles rather than extracting profiles (Figure 7a) to avoid spurious artifacts. East-west ramp is removed by picking latitudinal profiles and detrending.

The latitude-longitude position of the deepest points in the graben system which is assumed to be the graben's strike direction is shown in Figure 8a. The depth of each of these points is plotted in Figure 8b. Depth is calculated by fitting a line (by the least mean square method) over the topographic profile perpendicular to the graben strike, subtracting the height of the line from the actual depth of the graben at the same x-y point. Approximate width of the graben at each of the points shown in Figure 8a is plotted in Figure 8c and slope in Figure 8d, i.e. along the strike of the graben. The erratic distribution could be attributed to small residual features as opposed to representing the regional trend. Slope is calculated by half width by depth.

The system can be supposed to have two types of asymmetry- along strike and across strike (complicated by a ramp-topography of the area). A fault dominated model was attempted to explain the cross strike asymmetry. Since it does not yield convincing results, it is detrended and assumed symmetrical for the time being.

## **MODELING**

Boundary element method is used to run forward models using POLY3D, which is a C language computer program that calculates displacements, strains and stresses induced in an elastic whole or half space by planar, polygonal-shaped elements of displacement discontinuity. Boundary conditions can take the form of either relative displacements or tractions. Poly3d has been modified to account for gravitational body forces in a manner similar to its two-dimensional counterpart TWODD [Martel, 2000]. The polygonal element represents some part of the fracture or fault surface which acts as the source. The displacement field is continuous everywhere except

across the element itself. Boundary conditions can be burger vectors or traction (from which burger vectors are calculated) or mixed mode. (Figure 9a)

Angular dislocation is a linear function of the three Burgers vector components where the  $U_{ij}$  are *displacement influence coefficients for the angular dislocation*..

$$u_i = U_{ij}(\underline{x}; \xi, \beta, \omega) b_j$$

More specifically  $U_{ij}$  gives the displacement component,  $u_i$ , at position,  $\mathbf{x}$ , resulting from a Burgers vector component,  $b_j$ , of unit magnitude on an angular dislocation defined by  $\xi$ ,  $\beta$ , and  $\omega$ .  $U_{ij}$  is directly related to strain influence coefficients  $E_{ijk}$  by:

$$E_{ijk} = \frac{1}{2} \left( \frac{\partial U_{ik}}{\partial x_j} + \frac{\partial U_{jk}}{\partial x_i} \right)$$

In general, an N-sided polygon requires 2N angular dislocations, so the total displacement field is given by:

$$u_i = \sum_{n=1}^{2N} U_{ij}^n b_j$$

Stress is related to strain via Hooke's Law:

$$\sigma_{ij} = 2\mu\varepsilon_{ij} + \lambda\varepsilon_{nn}\delta_{ij}$$

$$S'_{ijk} = 2\mu E'_{ijk} + \lambda E'_{nnk}\delta_{ij}$$

where  $\mu$  is the shear modulus,  $\lambda$  is Lamé's lambda,  $\delta_{ij}$  is the Kronecker delta, where  $\mathbf{S}$  are the stress influence coefficients for an N-sided polygonal element. Hence, via boundary element modeling displacements can be calculated from burger vectors/boundary tractions and from the displacements, stress and strains may also be calculated.

The input parameters required are the physical parameter constants, the coordinate systems for all the calculations, exact geometry of the source in the form of coordinates of all vertices of the elements (numbered correctly) and orientation with respect to each other in the case of multiple sources, observation grids and stress conditions. A Matlab GUI is used to define the input parameters (modified and rewritten to suit this particular problem), which is mixed into the C code. A planar geometrical approach is shown in Figure 9b. The output file gives the displacements, stresses and principal stresses at each point on the observation grid.

The analysis was initiated using a simple graben modeled by two normal faults dipping toward each other with a dike intrusion at the base (Figure 10). The dike is forced to have a tensile opening (uniform) while linearly increasing the hydrostatic stress at the rate of 8.162 MPa/km with depth. This calculation is done using simple

hydrostatic pressure ( $g = 3.71\text{m/s}^2$ ) exerted by the magma chamber over a particular depth. Density of magma varies with depth but using the model from *Wilson and Head, 2002* a uniform density of  $2200\text{ km/m}^3$  is adopted (Figure 10). The normal faults have zero stress conditions. These conditions are maintained for the following models too. A number of such forward models were run, changing sequentially the input parameters to observe the effect on the surface displacements. The aim is to decide on a suitable starting model for the fault-dike system which causes displacements similar to the ones that can plausibly cause the observed Martian topography. This starting model can then be used to run a 3D inversion to solve for the displacement discontinuities which caused this topography. Knowledge of the source geometry and intensity can give us valuable information about the mechanism of development of this geological feature. This can prove to be important because there is a dense grid of tension cracks immediately east of this deepening graben system, a feature speculated to be an indicator of fluvial systems.

The input parameters that were varied are:

- Basic source geometry (two normal faults and an intrusive dike, a dike intruding an asymmetric normal fault, a single normal fault causing a tensile opening, the graben-dike system with a cylindrical magma intrusion on one side, dike intrusion whose horizontal extent exceeds the normal faults, plunging normal faults with a dike intrusion)
- Dip of the graben
- Dip of the dike
- Ratio of the depth of the graben with respect to depth of dike
- Vertical separation between graben and magma intrusion
- Horizontal separation between the 2 legs of normal faults
- Along-strike length of the fault-dike system to check edge effects and the displacement-length ratio (which is an indicator of mechanical restriction at depth)
- Stress conditions (horizontally varying linearly, vertically varying linearly, constant throughout)

The effect of the above modeling changes are shown in Figure 11 a-e with detailed explanations alongside the figures. Although, this process provided valuable insight into the kind of source needed to match the profile of the graben shoulders, none of the dike-graben simple structures could explain the asymmetry in depth of the data. To bring in the asymmetry, the tensile opening was forced to vary linearly along strike, however that increased upthrow rather than increase depth. A cylindrical intrusion was included on one end, which again did not cause the effect needed. The

cylinder represents the upwelling of a thin magma chamber that is the source of stress that spreads horizontally, along strike, to form the dike opening. Since the latter process has not been modeled and added to the displacement solution, both the models show an unnaturally high and sudden positive displacement at the point where the stress is concentrated (Figure 12, 13). Although, both the above models do bring in an along-strike asymmetry but we resorted to a plunging graben system to explain the asymmetry seen in the data.

As the length increased, the displacement to length ratio increased slightly then continued indicating that the faults are probably restricted by a mechanical boundary [Polit et al, 2005]. However, if a segmented echelon geometry exists [Goudy & Schultz, 2005], lower than expected ratios may be measured. Hence, length ratios do not seem to be a very dependable factor to constrain crustal dichotomy, at least in this area (Figure 11d).

### **PLUNGING GRABEN SYSTEM**

The along-strike asymmetry was modeled using a pair of normal faults which dipped toward each other and along plunged along-strike leading to a smoothly plunging graben with a dike intrusion at its base. This system is modeled using trapeziums as the normal faults and the dike as opposed to rectangular sections as before. The geometrical controls for each trapezium are as follows: [1] Strike  $\phi$  (width of the graben opening), [2] Dip  $\psi$  (Steepness of the graben), [3] Trapezium angle  $\theta$  (marked in Figure 14), [4] Plunge of the normal fault contact P, [5] Length of the trapezium sides L(asymmetry of plunge), [6] Depth at which the graben begins h, [7] Width of the graben W(surface horizontal extent of the feature). Out of the 4 angles, only 2 are independent so as to make the 2 trapeziums touch each other to form a graben with the plunging edge CB and edge DA at the Martian surface as shown in Figure 14. The dike intrusion touches the base of the graben, CB. The angle of ABCDA with the vertical is the dip and the angle DEC in the side view is the plunge P. To, find the exact relations between the 7 parameters in terms of the 3 independent terms, the following equations are used:

$$\tan(\phi) = \frac{FB * \cos(\psi)}{EF}$$

$$\sin(P) = \frac{FB * \sin(\psi)}{EB}$$

$$h = L * \sin(\theta) * \sin(\psi)$$

These equations eventually simplify to:

$$\cos(\psi) = \tan(\theta) * \tan(\varphi) \quad \dots \text{Eq (1)}$$

$$\sin(P) = \sin(\psi) * \cos(\theta) \quad \dots \text{Eq (2)}$$

$$h = L * \sin(\theta) * \sin(\psi) \quad \dots \text{Eq (3)}$$

Evidently, for any model, at most 2 of the angles, one among  $h$  and  $L$  to determine the size of the fault sides and width of the faults ( $W$  for horizontal extent) can be specified. The angular dependence can be clearly seen in Figure 15. The dike is also modeled as a trapezium whose  $\theta$  is equal to  $(90-P)$ ,  $P$  being the plunge of the graben system. The length  $L$  of the dike is chosen according to how deep it needs to be, width in accordance to width of the graben (since lateral extension causes artifacts seen in Fig. 11) and the strike being the average of the strikes of the normal faults. Once these parameters are determined, the polygonal elements used to model the shapes are a combination of rectangular and trapezoidal. All the vertices and element numbers are calculated and fed into poly3d for forward modeling.

From modeling experiments using the plunging model and stress conditions as before, the following facts are inferred:

- The cross-graben vertical displacement solution shows a graben width similar to the distance between the normal faults at the surface at that point. In other words, the strike does not change from model to solution (Figure 16a). This is a decisive factor and is kept as an independent variable.
- Plunge of the actual displacement solution is about 5 orders of magnitude less than the plunge of the source model (Figure 16b). Hence, this is not a decisive factor and can be kept as a dependent variable.
- The graben walls in actual displacement solution are much steeper than those of the source model (Figure 16a). Also, as proven in Figure 11a, as the dip of the model faults decreases, the solution graben walls become steeper. This is a decisive factor and is kept as an independent variable.
- Trapezium angle must be very large, i.e. the normal fault segments should be almost rectangular in order to avoid unrealistic solutions resulting from models like in Figure 16c. From Figure 15, high  $\theta$  agrees with the calculations that strike should be very low when dip is high. Hence, it is safe to keep this variable as dependent on dip and strike.

To calculate the strike, the data distribution (Figure 8) is used which shows width to vary from 3km to 6km approximately over a graben length of  $\sim 150$ km. From Figure 17, strike  $\sim 1$  degree. Since such a small value is giving rise to artifacts, strike is approximated to be 2 degrees. Data also shows dip of 70-80 degrees, hence model dip

should be higher, eventually selected as 85 degrees. The final model (scaled down in distance) and vertical displacement solution is shown in Figure 18. As expected, an along-strike asymmetry is seen while maintaining graben formation and as the faults in the model (above) widen and deepen, the graben in the solution widens and shallows out due to the dike going further away from the surface.

## RESULTS AND CONCLUSION

Since detrending the topography removed the cross-graben asymmetry considerably, the modeling concentrates on attempting to explain the along-graben asymmetry. Individual profiles cutting across the graben (MOLA profiles) are compared with profiles extracted from the POLY3D solution on the 2D observation grid, at similar points along the graben. The results are shown in Figure 19. In (A), the dike dip is almost 90 degrees hence the profile is symmetrical while in (B), cross-graben asymmetry is brought about by modeling the dike dipping at 75 degrees. Many of the profiles show that the cross-strike topographic profile of a graben is asymmetric, i.e., one side is concave-up and the other side is concave-down (Figure 6). This asymmetric profile is attributed to unequal fault dips and offset magnitudes on either side of the graben [e.g., *Rubin, 1992; Schultz et al., 2004*].

Figure 20 compares the along-graben profile of Martian topography data (red curve) and the plunging model vertical displacement solution (blue curve). The model (strike divergence of normal faults = 2 degrees, dip of faults = 85 degrees, plunge = 25.74 degrees) plunges from left to right and the deepest point is approximately at X=0, Y=150 km as shown in Figure 18. The strike is forced to match the width of the graben varying from 2.5km to 6 km. The vertical displacements caused by the plunging model do deepen but exponential decrease in topography is only possible if, at the deepest point of displacement solution, the tensile extensive stress is high enough to cause a pit crater to form. The tensile component of stress along the graben is calculated by adding the X-components of the 3 principal stresses. A scaled version is plotted as the black curve in (A) and the actual version (for unit tensile boundary condition on the dike) in (B). The graben is along the Y-axis so the tensile opening will be along X. It is maximum toward the beginning of the profile where vertical displacement is maximum, i.e. the point at which the dike is closest to the ground surface. This increase in extensive tensile component due to the plunging model may lead to the formation of a large pit crater at the deepening end of the graben, as seen in the data. Further along the strike, the tensile stress component decreases hence the depth of the pit craters decrease. This is clearly seen in the MOC images in Figure 21.

The offset between the two grabens as seen at 266.15 deg longitude and 22.3 deg latitude in Figure 8a, can be explained by a segmented fault-dike system as shown in Figure 22. The system to the west of the offset does not seem to be a plunging system because the depth of the graben along that segment is uniform (corresponds to the segment between 25 km to 70 km along profile in Figure 8b). The system to the east of the offset is proven to be a plunging system from east to west, as described earlier, with varying dike dip and offset to explain the variation in cross-graben symmetry. As the graben continues eastward, the extensive (negative) stress increases in the cross-graben (along X-axis) direction and beyond a particular point causes pit crater to open up. We see this in the DEM topography as a deepening graben culminating in a very deep pit crater. The formation of this structure relieves the strain considerably and the pit crater chain following along the same strike, decreases in depth toward the east.

## **FUTURE WORK**

The work done in the project was an initiation to the approach of intertwining Poly3d modeling and data from MOC, THEMIS and MOLA in order to explain the formation of the structures at Alba Patera. A candidate site was selected for the same, the approach applied and an approximate explanation cited. In order to justify the purpose of the project, more such sites will be selected, modeled and a pervasive mechanism suggested for the formation of the Tharsis graben and pit crater chains.

## **ACKNOWLEDGEMENTS**

This research was carried out at the Jet Propulsion Laboratory, California Institute of Technology, and was sponsored by NASA PGGURP and the National Aeronautics and Space Administration. I would like to express my deepest sense of gratitude to my supervisor, Dr. Paul Lundgren for expert guidance and support throughout the project work, Dr. Steve Martel for valuable insight into the problem, the JPL/Beacon and the CalTech SFL for the huge amount of reading material and the Student Faculty Programs Office and the PGGURP Committee for making this trip, halfway across the Globe, possible not only in terms of excellent research experience, the greatest friends and an opportune career launcher but also for allowing me a wonderful summer-full of memories to take home with me.

## **REFERENCES**

Cailleau, Beatrice et al, Unveiling the origin of radial grabens on Alba Patera volcano by finite element modeling, *Icarus*, Volume 176, Issue 1, p. 44-56, 07/2005.

Ferrill, David et al, Dilational fault slip and pit chain formation on Mars, *GSA Today*, pp. 4-12, DOI: 10.1130/1052-5173(2004)014

Gaddis, L. et al, High-resolution topography of layers in the Valles Marineris via 'Thermoclinimetry', Thirty-Sixth Lunar and Planetary Science Conference, 2005

Goudy, Cheryl L., Schultz, Richard A., Dike intrusions beneath grabens south of Arsia Mons, Mars, *Geophy. Research Letters*, VOL. 32, L05201, doi:10.1029/2004GL021977, 2005

Kirk, R.L. et al, High-resolution topomapping of candidate MER landing sites with Mars Orbiter Camera narrow-angle images, *Journal of Geophysical Research*, Volume 108, Issue E12, pp. ROV 29-1, 12/2003.

Martel, S.J, Muller, J.R, A Two-dimensional Boundary Element Method for Calculating Elastic Gravitational Stresses in Slopes, *Pure and Applied Geophysics*, Volume 157, Issue 6-8, pp. 989-1007 (2000).

Neumann, G. A., M. T. Zuber, M. A. Wieczorek, P. J. McGovern, F. G. Lemoine, and D. E. Smith, Crustal structure of Mars from gravity and topography, *J. Geophys. Res.*, 109, E08002, doi:10.1029/2004JE002262, 2004.

Okada, Yoshimitsu, Surface deformation due to shear and tensile faults in a half-space, *Bulletin of the Seismological Society of America*; August 1985; v. 75; no. 4; p. 1135-1154

Okubo, C. H., and S. J. Martel, Pit crater formation on Kilauea volcano, Hawaii, *J. Volcanol. Geotherm. Res.*, 86, 1-18, 1998.

Okubo, C. H.; Schultz, R. A., Evidence of Tharsis radial dike intrusion in Southeast Alba Patera from MOLA-based Topography of Pit Crater Chains, 36<sup>th</sup> Annual Lunar and Planetary Science Conference, March 14-18, 2005, in League City, Texas

Okubo CH, Schultz RA, Evidence Of Normal Faulting And Dike Intrusion At Valles Marineris From Pit Crater Topography, Thirty-Sixth Lunar and Planetary Science Conference, 2005

Okubo, C. H. et al, Gridding Mars Orbiter Laser Altimeter data with GMT: effects of pixel size and interpolation methods on DEM integrity, *Computers & Geosciences*, Volume 30, Issue 1, February 2004, Pages 59-72

Polit, A. T. et al, A Tale of Two Stratigraphies: From Alba Patera to the Northern Plains, 36<sup>th</sup> Annual Lunar and Planetary Science Conference, March 14-18, 2005, in League City, Texas

Roberts, G.P. et al, Possible evidence for on-going volcanism on Mars as suggested by thin, elliptical sheets of low-albedo particulate material around pits and fissures close to Cerberus Fossae, *Earth, Moon, and Planets*, Volume 101, Issue 1-2, pp. 1-16

Schultz, R.A., Lin, Jian, Three-dimensional normal faulting models of the Valles Marineris, Mars, and geodynamic implications, *Journal of Geophysical Research*, Volume 106, Issue B8, p. 16549-16566, 08/2001.

Schultz, R.A. et al, Igneous dikes on Mars revealed by Mars Orbiter Laser Altimeter topography, *Geology*; October 2004; v. 32; no. 10; p. 889-892; DOI: 10.1130/G20548.1

Schultz, R.A. et al, Revised model for simple planetary grabens and tectonic implications, Proceedings of the 31st Lunar and Planetary Science Conference, Lunar and Planetary Institute, Houston, 1990.

Tanaka, K. L., Tectonic History of the Alba Patera-Ceraunius Fossae region of Mars, Proceedings of the 20th Lunar and Planetary Science Conference, pp 515-523, Lunar and Planetary Institute, Houston, 1990.

Soderblom, L.A. et al, Accurate Fine-Scale Topography for the Martian South Polar Region from Combining MOLA Profiles and MOC NA Images, 33rd Annual Lunar and Planetary Science Conference, March 11-15, 2002, Houston, Texas

Thomas, A. L., POLY3D: A three-dimensional, polygonal element, displacement discontinuity boundary element computer program with application to fractures, faults and cavities in the Earth's crust, M.S. Thesis, Stanford University, 41 pp, 1993.

Wilson, L., and J. W. Head III, Tharsi-radial graben systems as the surface manifestation of plume-related dike intrusion complexes: Models and implications, *J. Geophys. Res.*, *107*, E8, 5057, doi:10.1029/2001JE001593, 2002.

Wyrick, D., D. A. Ferrill, A. P. Morris, S. L. Colton, and D. W. Sims, Distribution, morphology, and origins of Martian pit crater chains, *J. Geophys. Res.*, *109*, E06005, doi:10.1029/2004JE002240, 2004.

Zuber, M. T., The crust and mantle of Mars, *Nature*, *412*, 220-227, 2001.

Zuber, M. T., S. C. Solomon, R. J. Phillips, et al., Internal structure and early thermal evolution of Mars from Mars Global Surveyor topography and gravity, *Science*, *287*, 1788-1793, 2000.

# FIGURES AND TABLES

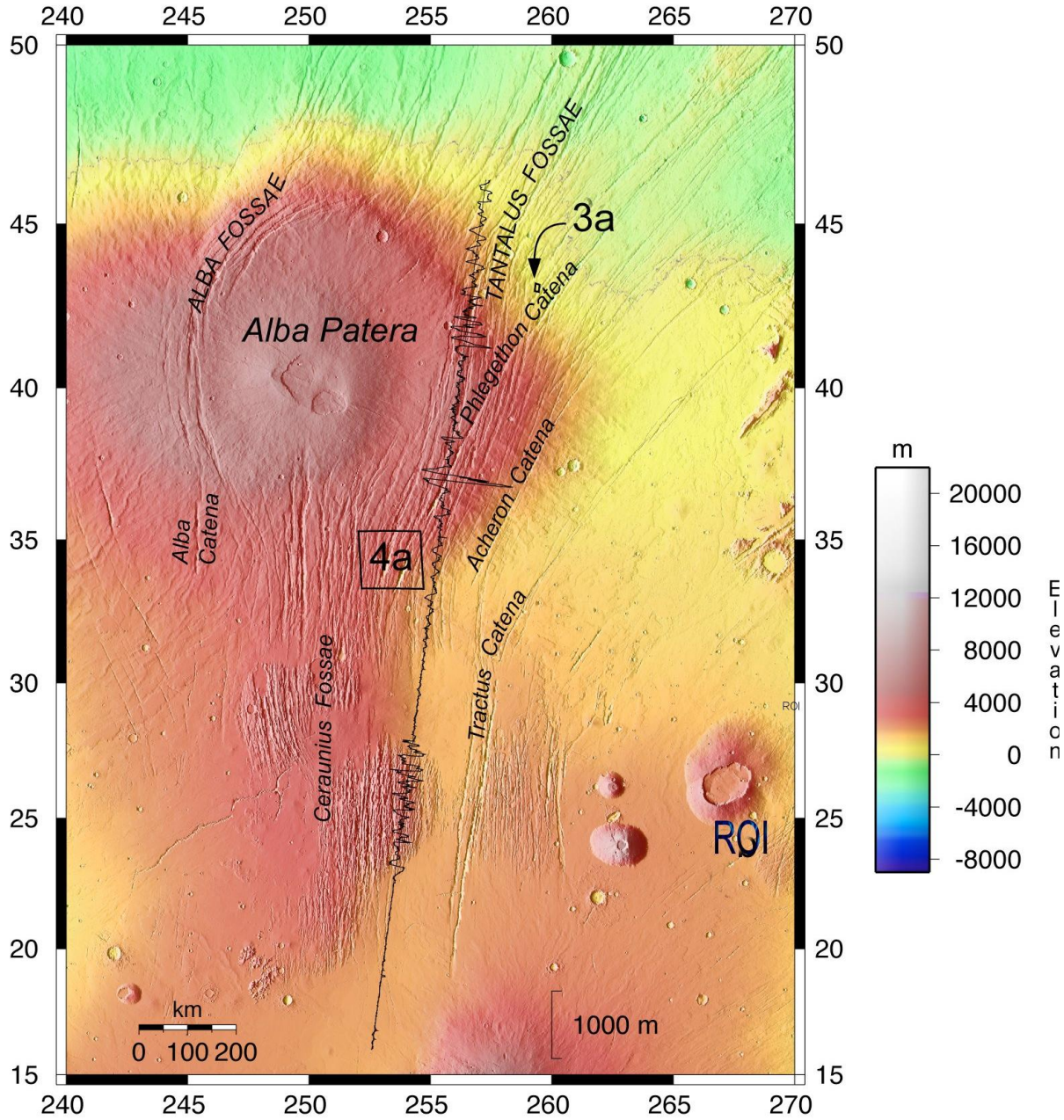


Figure 1: Topography from the MOLA MEGR database of the Alba Patera region. Black wiggly line is an example of a MOLA PEDR trace with its 1000 m vertical scale in lower right, and the map scale in the lower left.

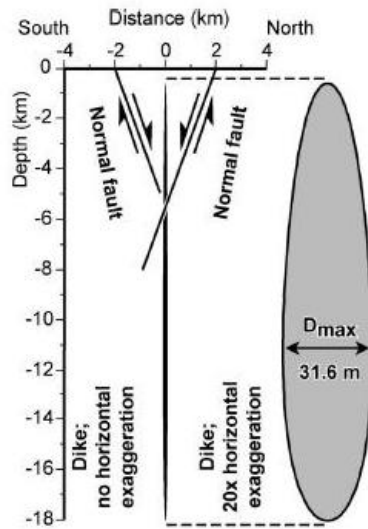


Figure 2a : Normal fault and dike geometry proposed in *Schultz et al, 2004* to explain the cross-sectional (symmetrical) profile of most of the Martian graben systems. The paper suggests that three consecutive events were necessary to produce the stress required to cause the observed deformation.

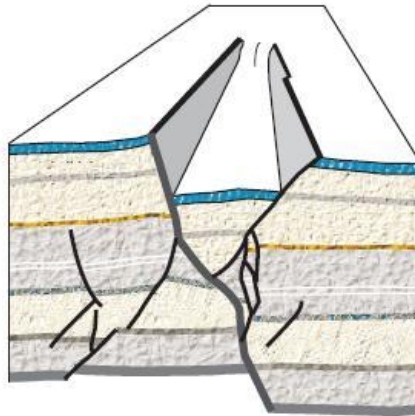


Figure 2b: The 'hourglass' model for surface-breaking planetary grabens as proposed in *Schultz et al, 2000*. The fault sets shown can retrodeform using dip-slip offsets.

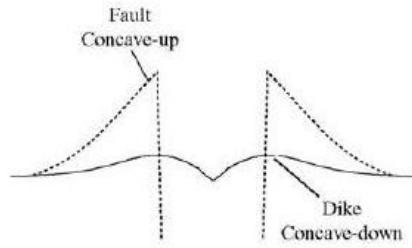


Figure 2c: A characteristic concave-up surface topographic profile produced by two normal faults and a concave-down topography produced by a dike intrusion. In a lot a cases, a mixed-mode is also observed.

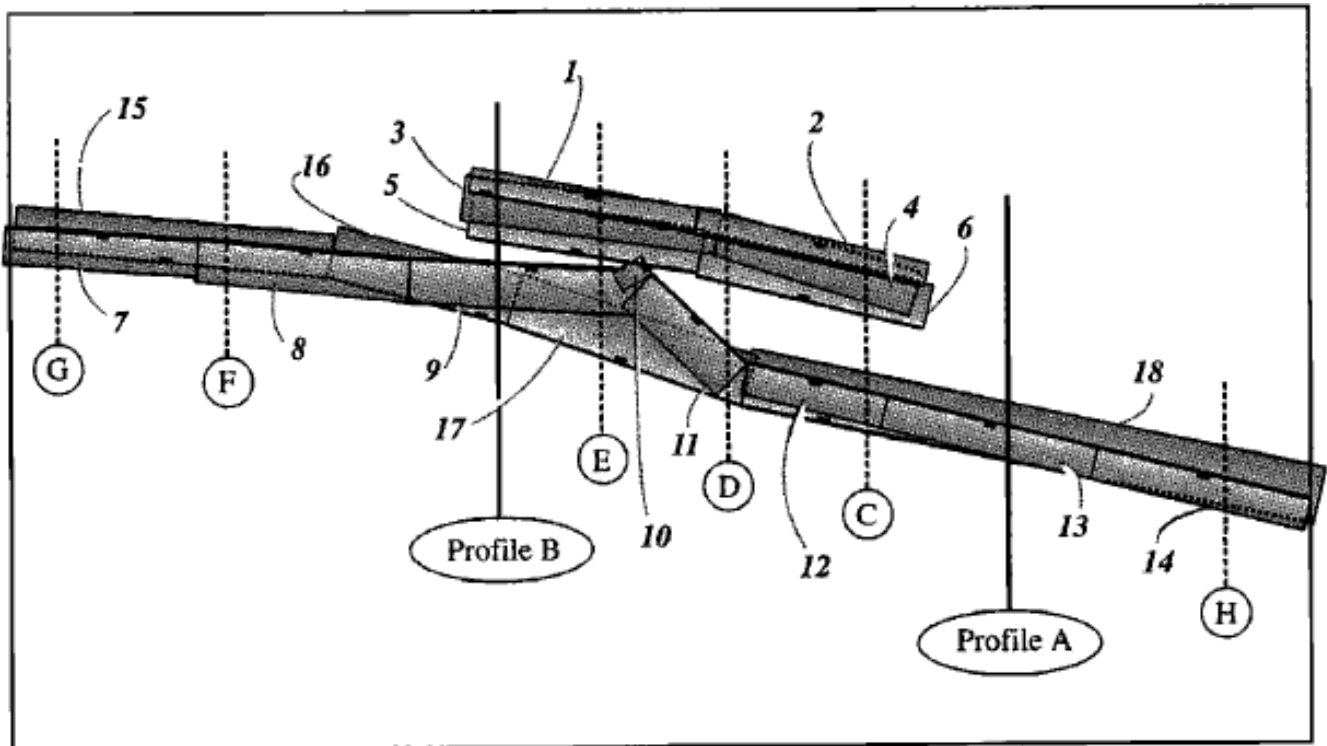


Figure 2d: Map showing fault geometries used in 3-D boundary element modeling of the entire trough system. Dashed curves show profiles for which individual BEM solutions were compared against MOLA topography; numbers denote the fault segments. Surface breaks of the segments are indicated by solid symbols on heavy curves. (Schultz and Lin 2001)

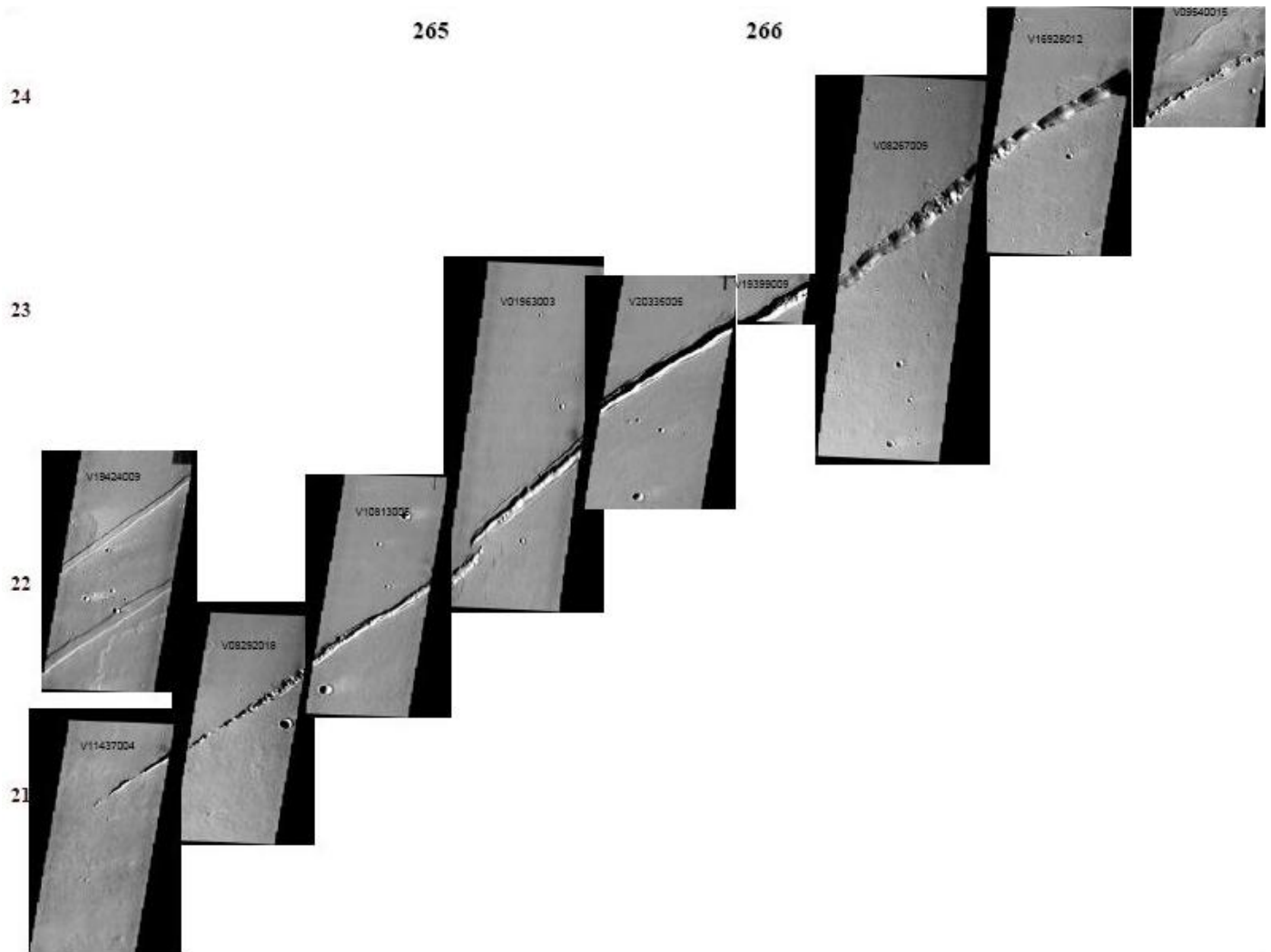


Figure 3a: Arrangement of THEMIS images (numbers marked within) of the graben/region of interest with the approximate latitude in degrees (Y axis), longitude in degrees (X axis) marked. The length of the feature, along strike, is about 240km.

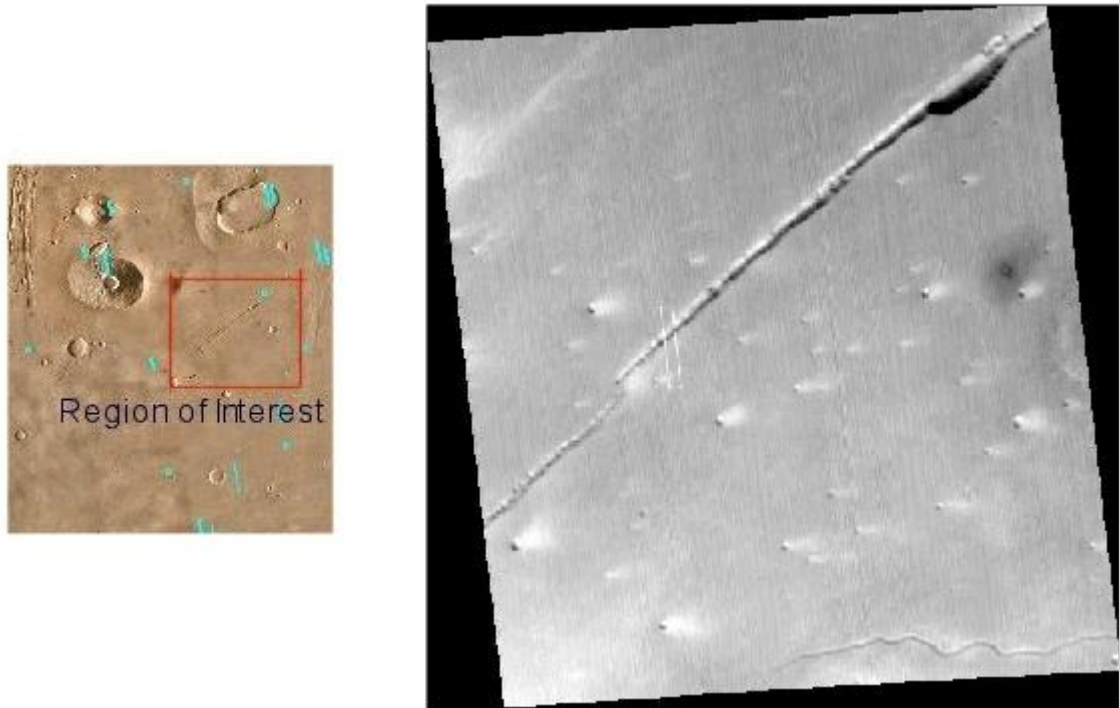


Figure 3b: [http://www.msss.com/moc\\_gallery/](http://www.msss.com/moc_gallery/) has the narrow and wide angle MOC images captured from 1999-2005. The view shown above is a small part of the Tharsis region which we chose as a candidate site. The blue spots, on the figure to the left are regions where the narrow angle MOC images are available. The figure to the right is the wide-angle MOC image (M14-00270) of the region of interest, height = 117.68 km and width = 121.55 km.

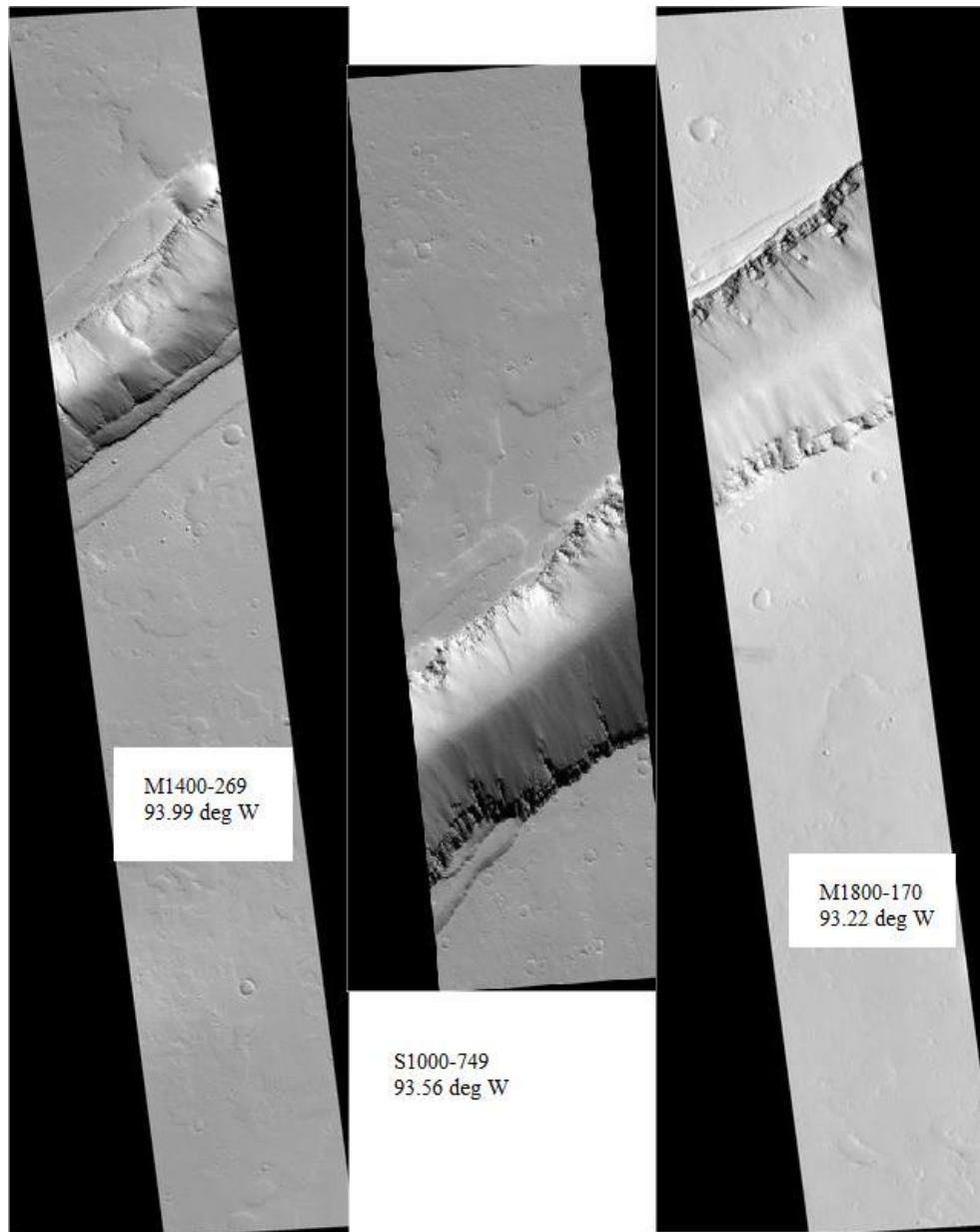


Figure 3c: A mural of 3 narrow angle images available from the MOC image archive as mentioned in Figure 3b's description. The longitudinal position and image number is mentioned alongwith. A deep graben system is clearly visible as in the THEMIS images.

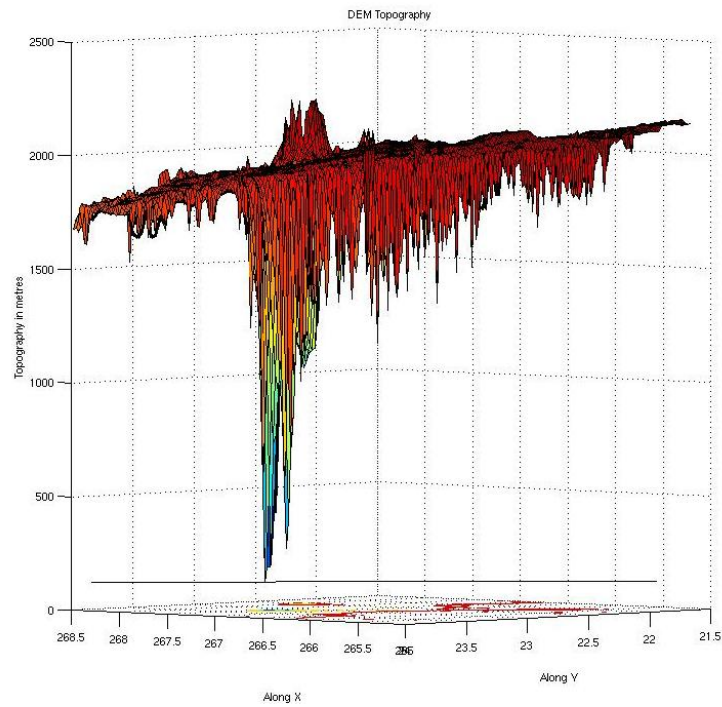
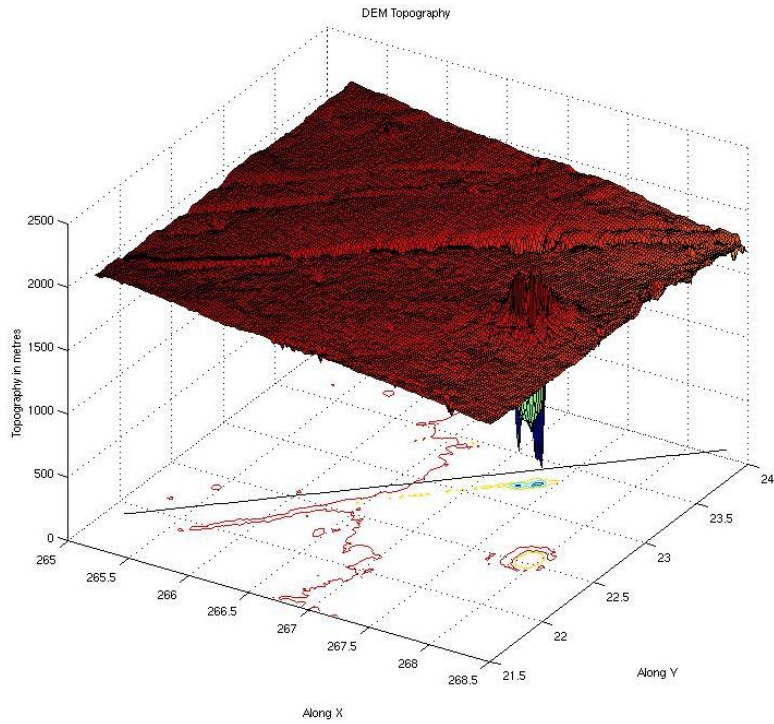


Figure 3d: The plan and cross-sectional view of the digital elevation model viewed 3-dimensionally in MATLAB via 'surf'. The deepening graben and the culmination in a crater stands out amidst the otherwise smooth topography.

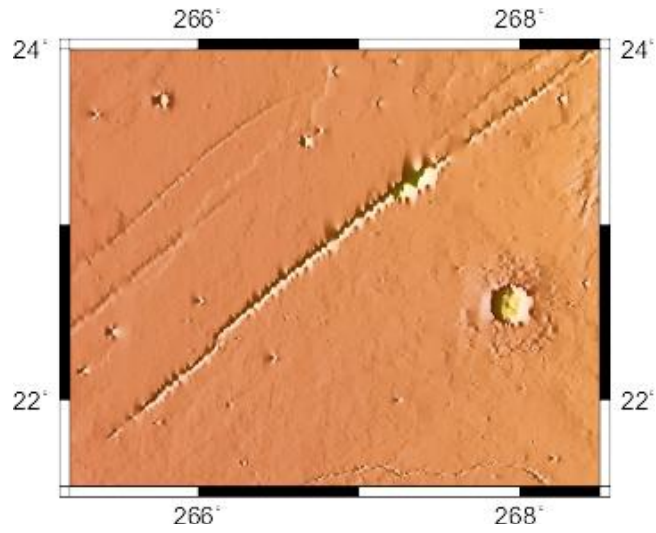


Figure 3e: GMT generated DEM of the region of interest. The feature to concentrate upon is the graben with a slight offset toward the west and culminating in a large crater toward the east.

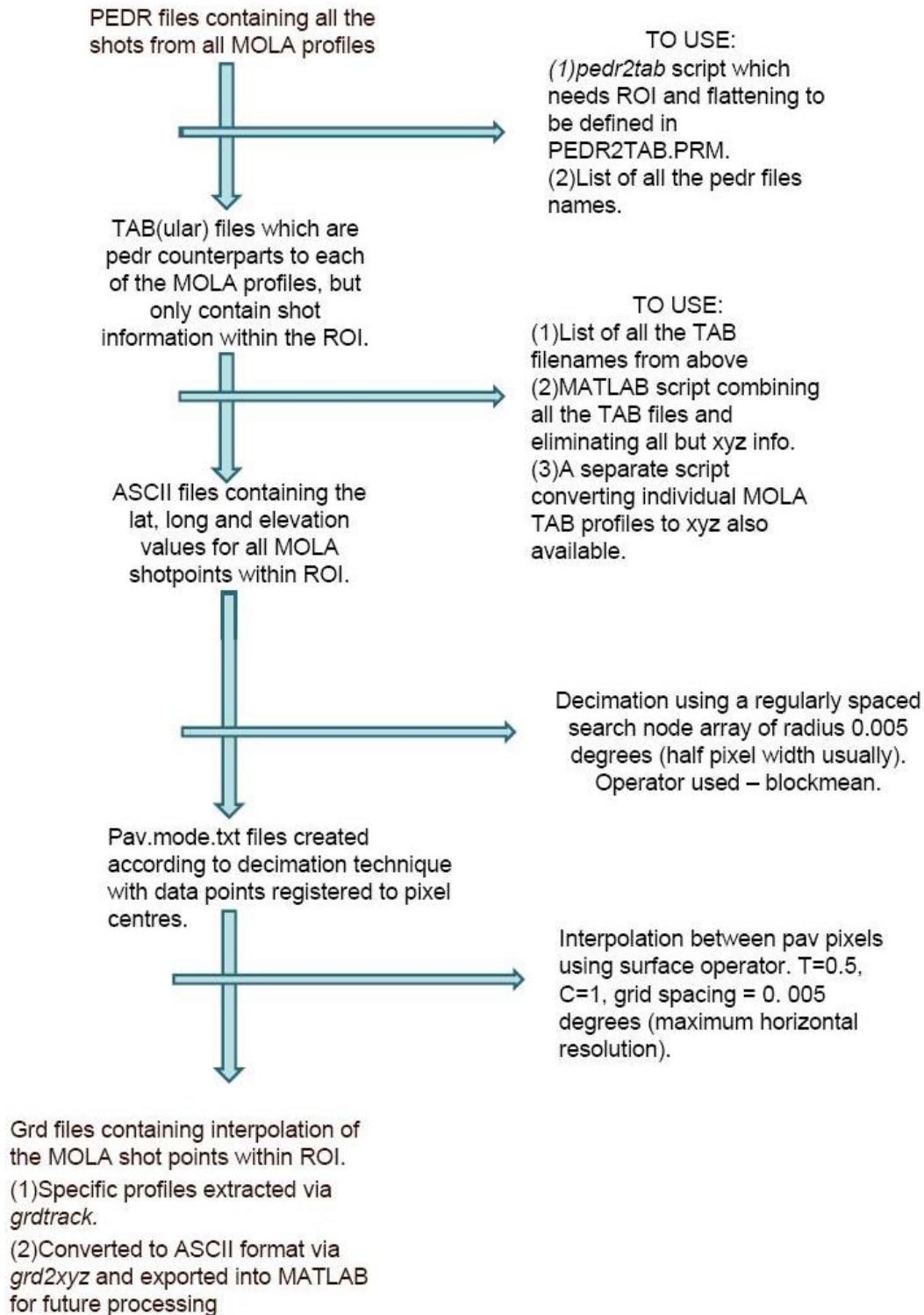


Figure 4: Flowchart showing the conversion of MOLA PEDRs to a MATLAB exportable DEM (left sequence). The files and parameters required for each step is indicated on the right side.

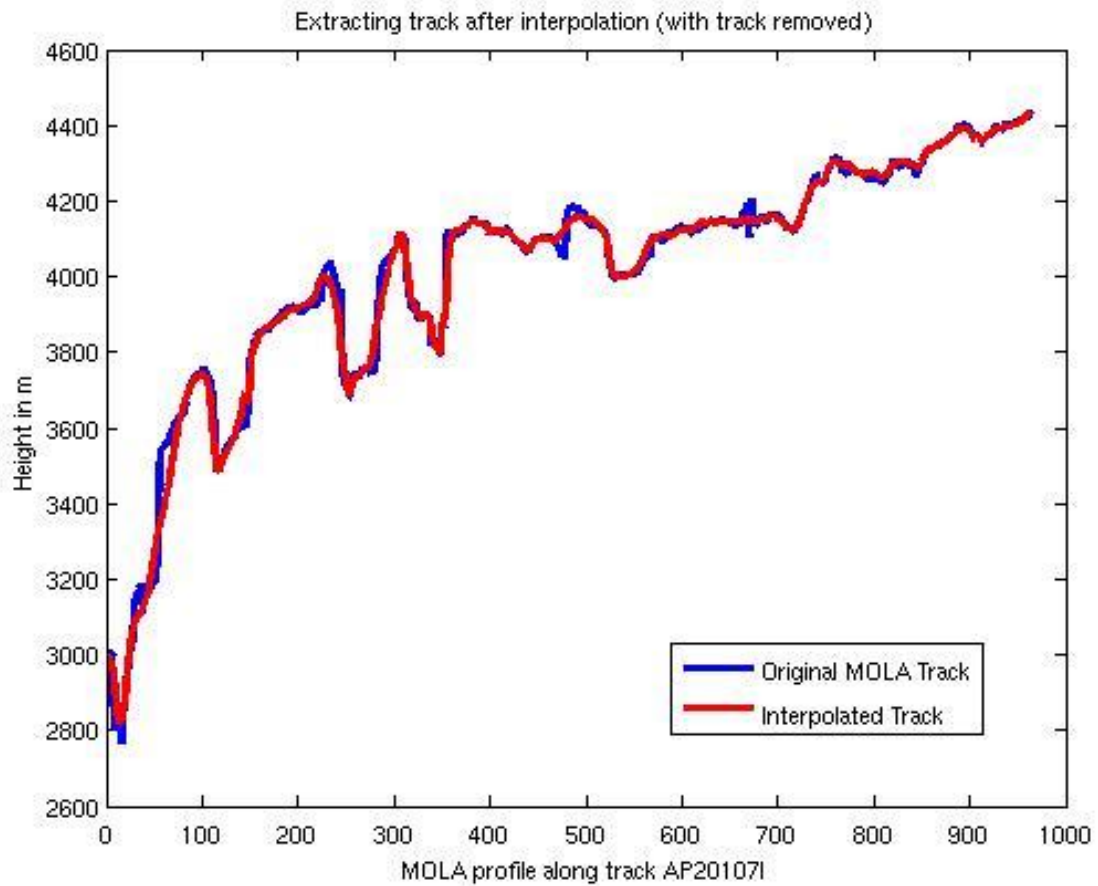


Figure 5: To check the interpolated quality of the data, the MOLA profile ap201071 was removed from the data, the rest of the profiles to interpolate the grid, GMT routine *grdtrack* used to extract the topography along the removed profile from the grid and compared with the original.

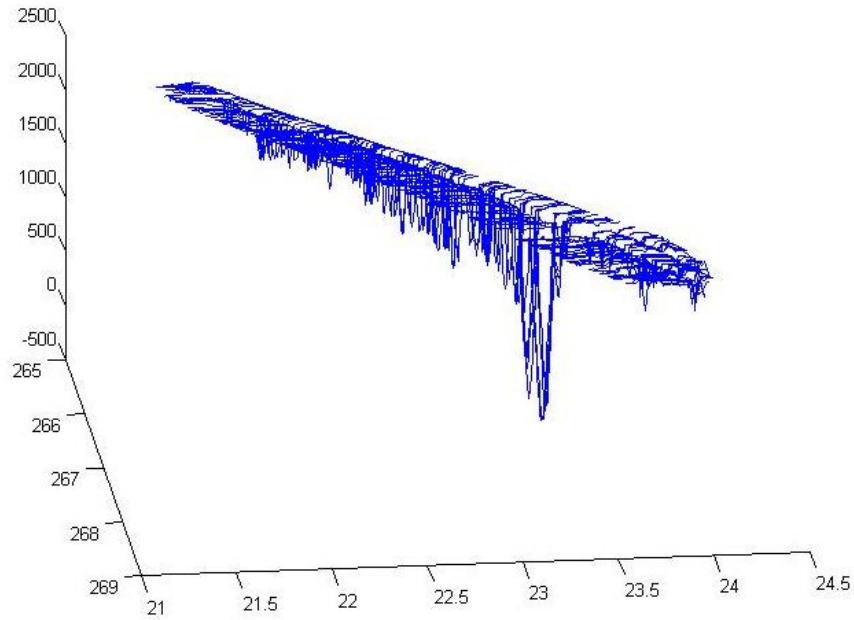


Figure 6: 129 MOLA profiles windowed within two parallel lines to constrain data within the graben system only.

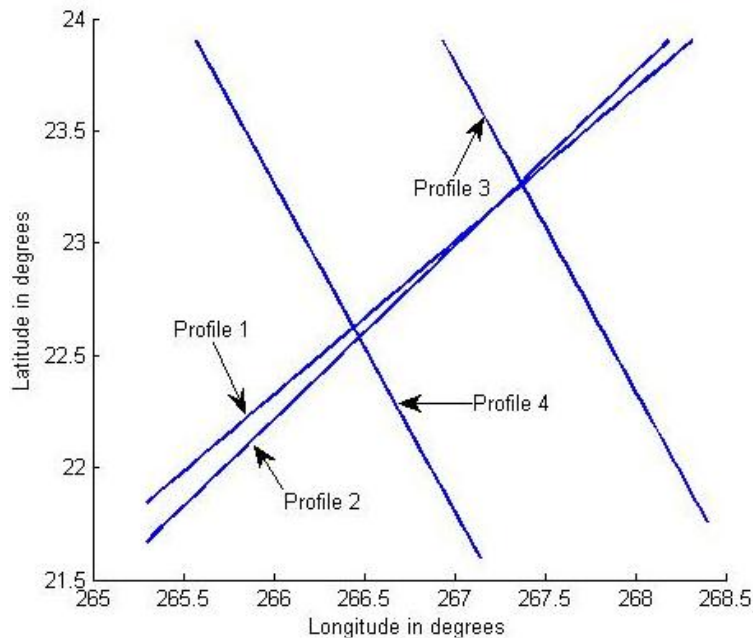


Figure 7a: Profile 1, 2 are lines fitted to the trend of the 2 parts of the graben strike and represent the along-strike profile. Profile 3, 4 are lines perpendicular to the first two, one of which passes through the deepest point in the graben. They represent the across-strike profile.

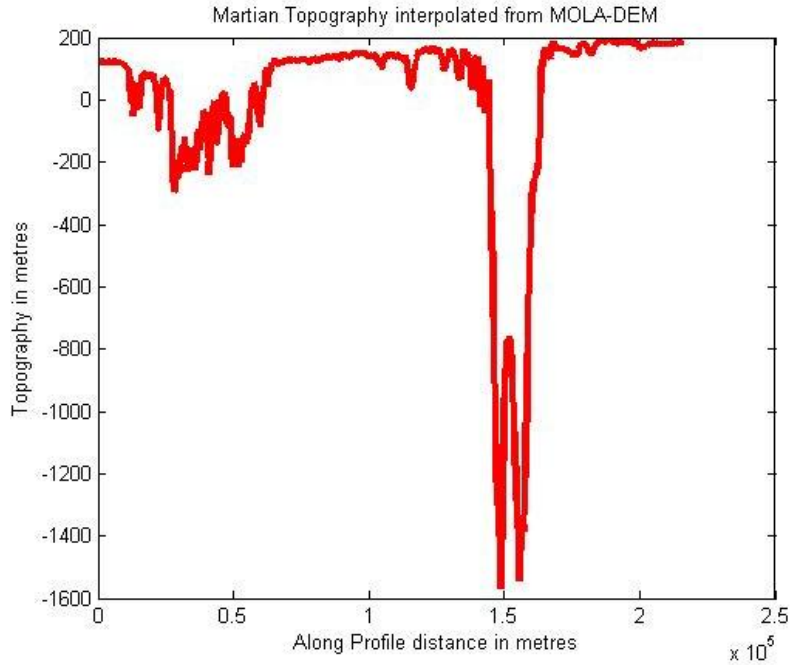


Figure 7b: Topography extracted from the gridded DEM along Profile 1. The sudden rise in topography within the deepest data points seems to be an interpolation artifact.

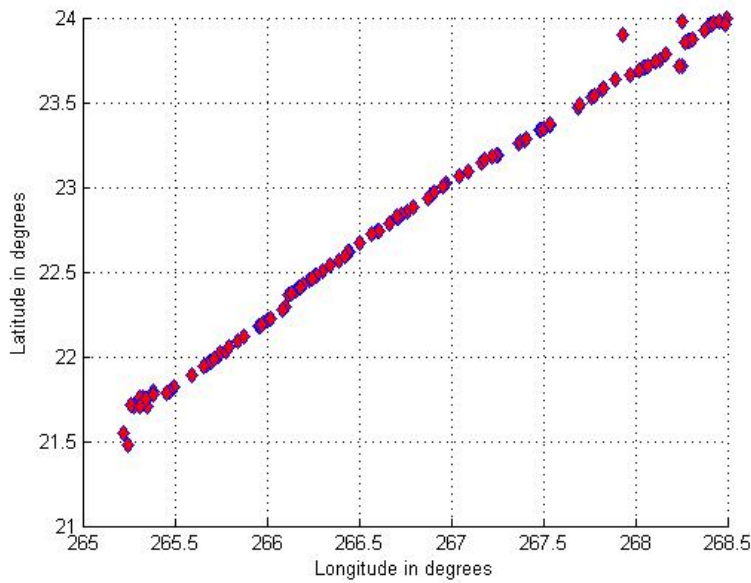


Figure 8a: The latitude-longitude position of the deepest points in the graben system which is assumed to be the graben's strike direction. The offset at longitude 266.15E

can clearly be seen. The deepest points were chosen from the MOLA profiles passing through the region of interest constrained within two parallel lines:  $\text{lat} = 0.7143 \cdot \text{long} - 168.1429$  and  $\text{lat} = 0.8333 \cdot \text{long} - 199.3333$ .

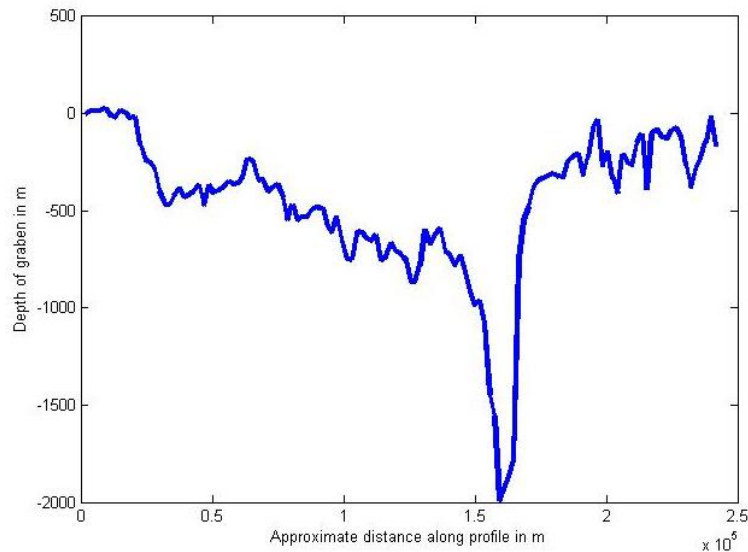


Figure 8b: A depth profile is plotted from the depth of the above points. Depth is calculated by fitting a line (by the least mean square method) over the topographic profile perpendicular to the graben strike, subtracting the height of the line from the actual depth of the graben at the same x-y point.

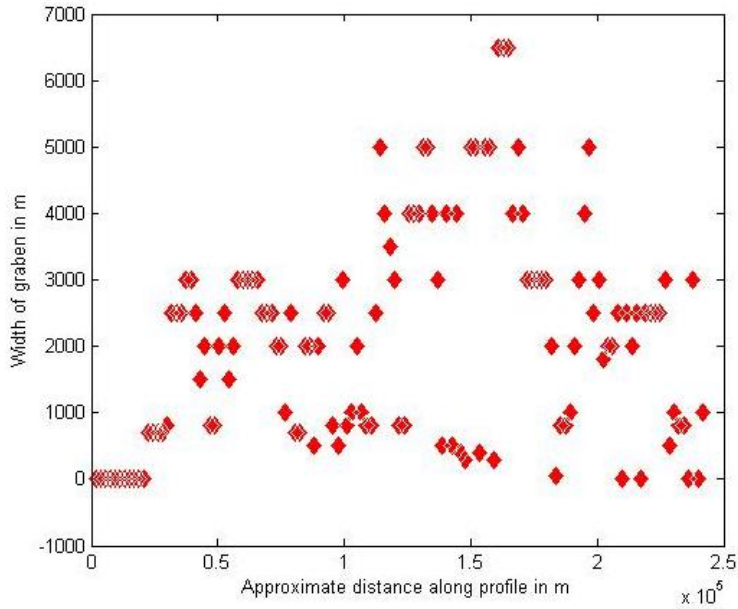


Figure 8c: Approximate width of the graben at each of the points shown in Figure 8a, i.e. along the strike of the graben. The erratic distribution could be attributed to small residual features as opposed to representing the regional trend.

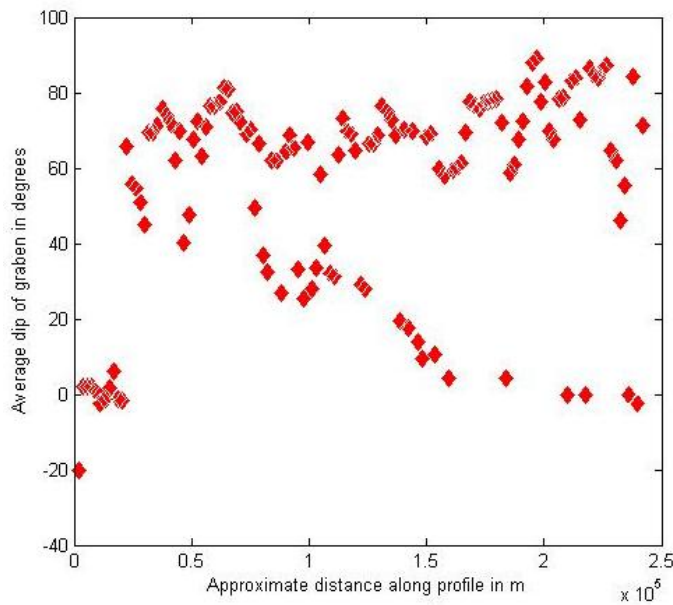


Figure 8d: Approximate slope of the graben at each of the points shown in Figure 8a calculated by half width by depth. The erratic distribution could be attributed to incoherences in width as explained above.

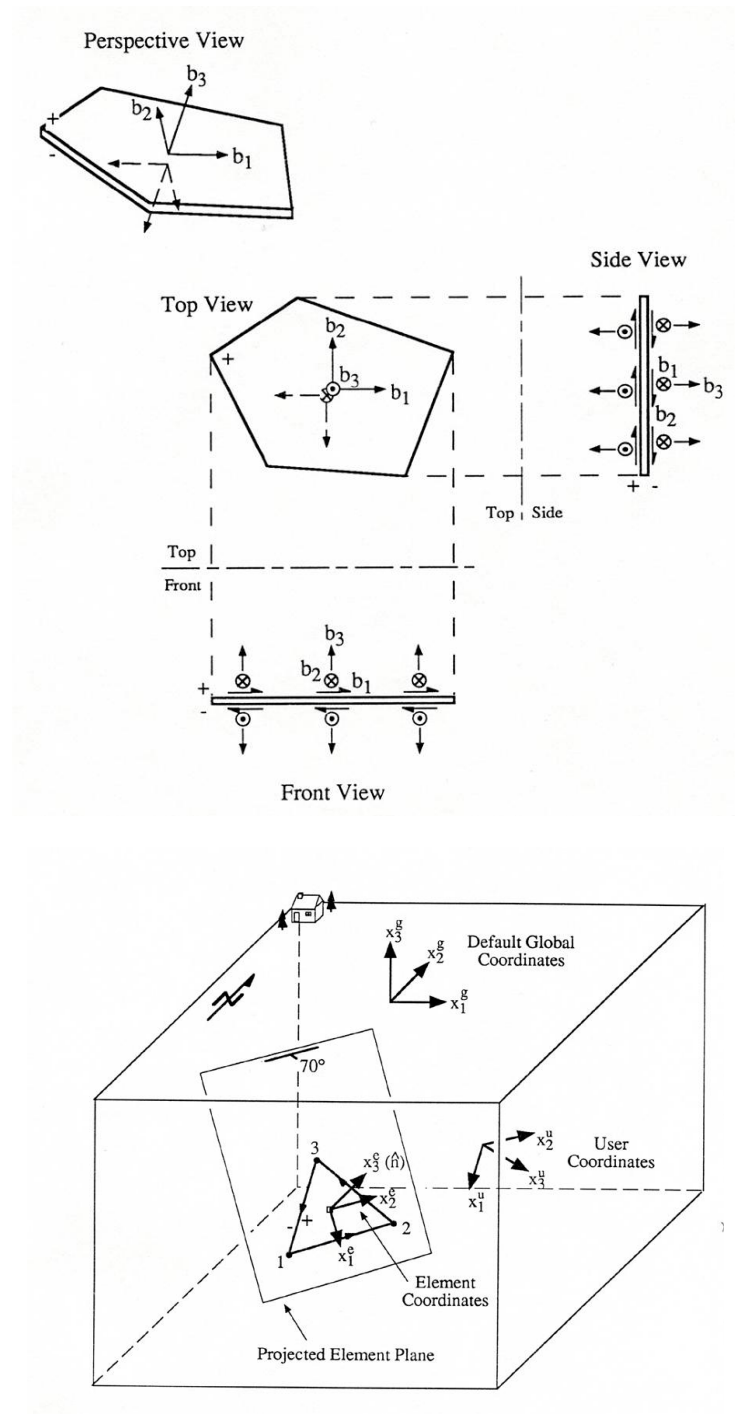


Figure 9a: As per *Thomas, 1993's PLOY3D code*, the polygonal element with the specified burger vectors is shown (top). An  $N$  sided polygon has  $2N$  angular dislocations. The elements are arranged onto the fault plane (below), coordinates specified and solution calculated at the observation grid specified – in our case ground surface.

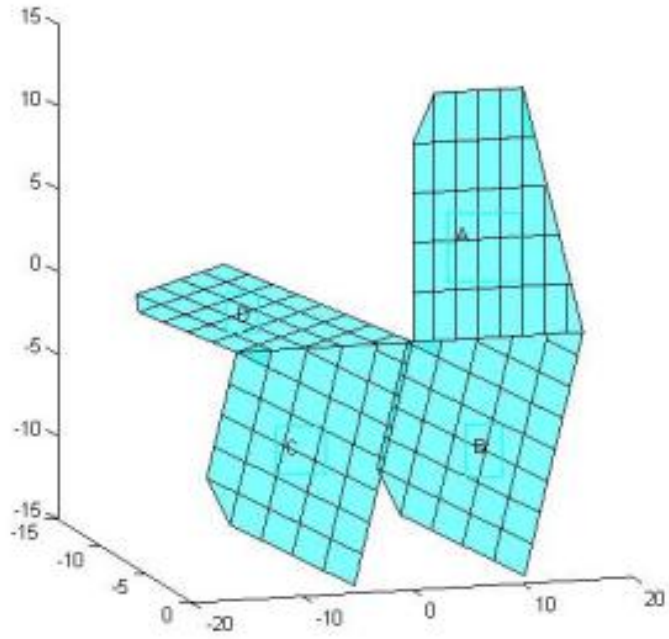
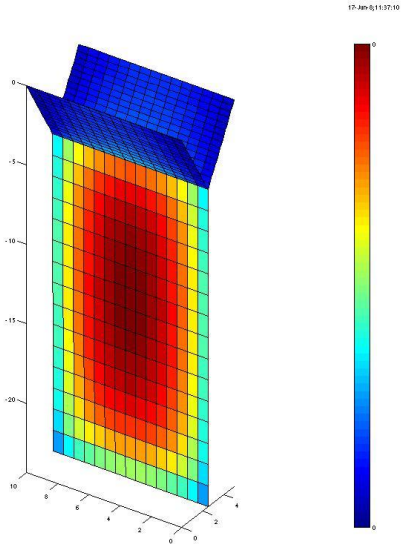


Figure 9b: The typical way to generate input parameters is to number and coordinate the vertices on a simple plane (Shape A) and rotate/translate it to the appropriate coordinates (Shape C), strike (Shape B, strike = 0) and dip (Shape D, dip = 10 degrees).



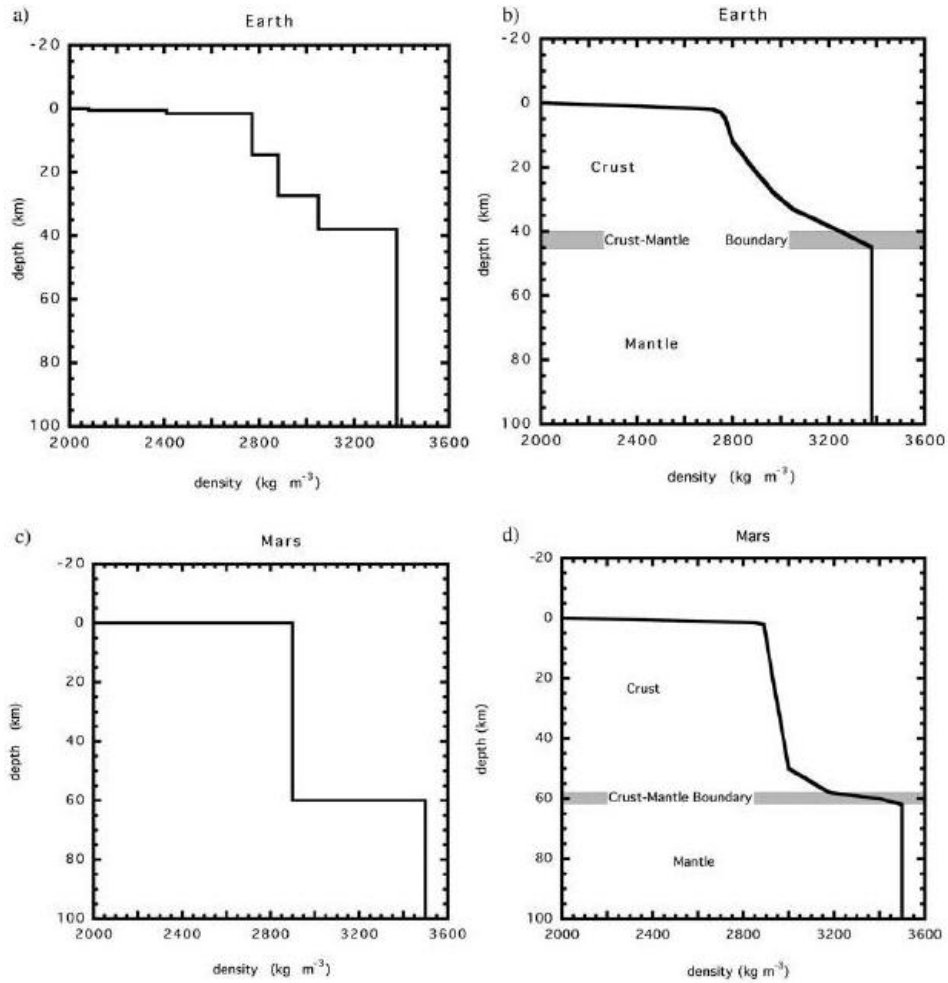


Figure 10: A simple graben modeled by two normal faults dipping toward each other with a dike intrusion at the base as proposed in *Schultz et al, 2004* (top). The colors represent the boundary stress conditions imposed on the proposed fault geometry. The dike is forced to have a tensile opening (uniform) while linearly the hydrostatic stress at the rate of 8.162 MPa/km with depth. The rate is calculated using density = 2200kg/m<sup>3</sup> from *Wilson and Head, 2002* (below). The normal faults have zero stress conditions. These stress conditions are maintained for the following models too.

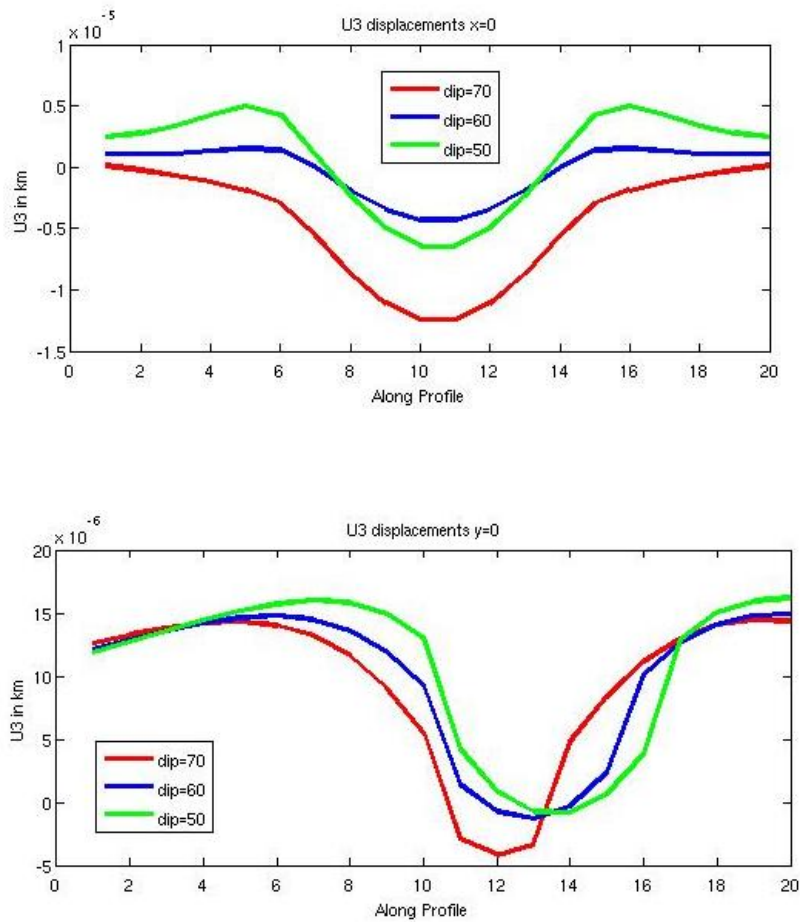


Figure 11a: The system in Figure 10 is tested with different dips of the normal faults, with the tip of the fault system being constant in space and the vertical ( $u_3$ ) displacement is plotted along two profile lines. Decreasing dip causes higher shoulders of the graben as seen in the cross-graben profile (top). Decreasing dip causes a flatter along-graben profile (down) where the deepest point will be at the centre of the graben system. Lower the dip, the closer the dike opening comes to the ground surface, hence more the upthrow.

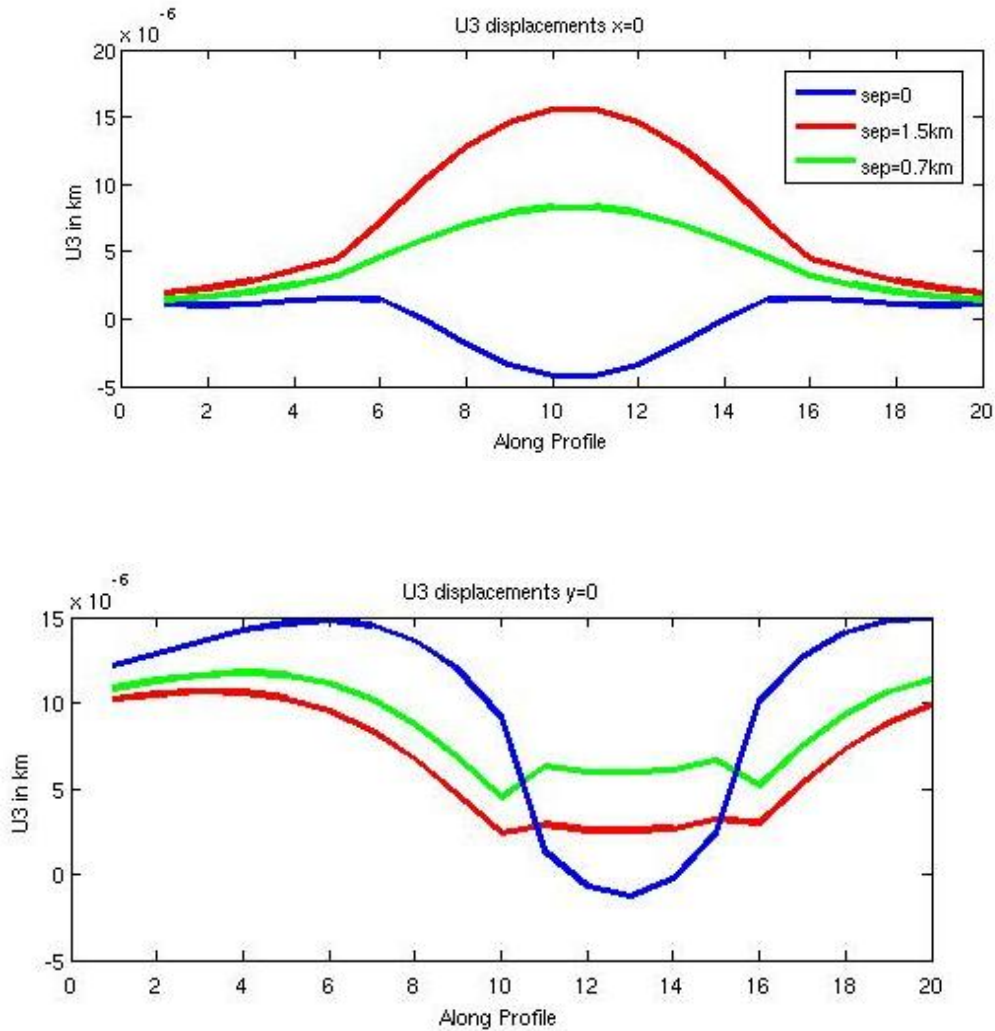


Figure 11b: The system in Figure 10 is tested with a horizontal gap (sep) between the normal faults, with the tip of the fault system being constant in space and the vertical ( $u_3$ ) displacement is plotted along an across graben profile line (top). Similarly, an isolated dike which has not reached the graben system is modeled (below) and cross-graben vertical displacement modeled. The depression seen the topography is primarily due to the dike opening as is obvious from the above experiments.

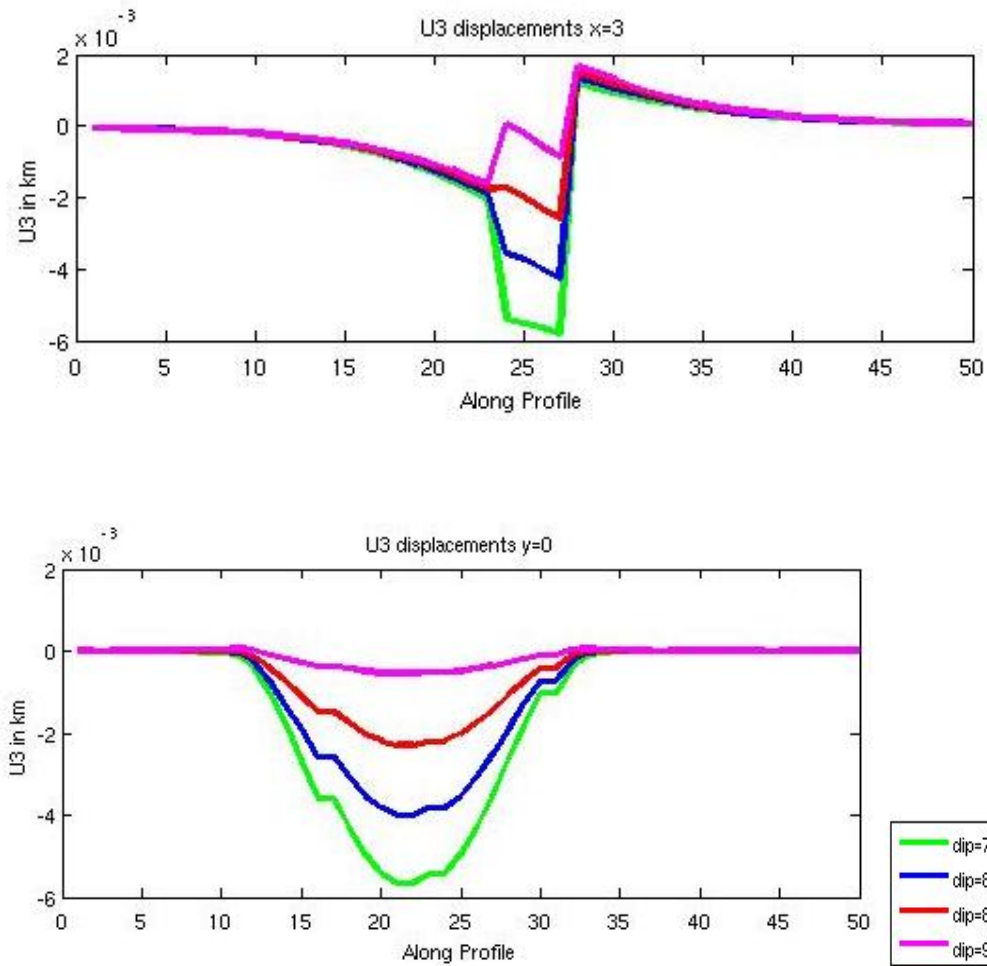


Figure 11c: Across strike asymmetry in figure 10's model is possible only if the dike has a dip (top). Less the dip, more the asymmetry – dip = 90 deg is modeled as 89.9 deg because poly3d cannot handle vertices directly below one another, hence the slight asymmetry. Along strike (bottom), symmetry is maintained and less the dip, closer the dike to the ground and more the displacement.

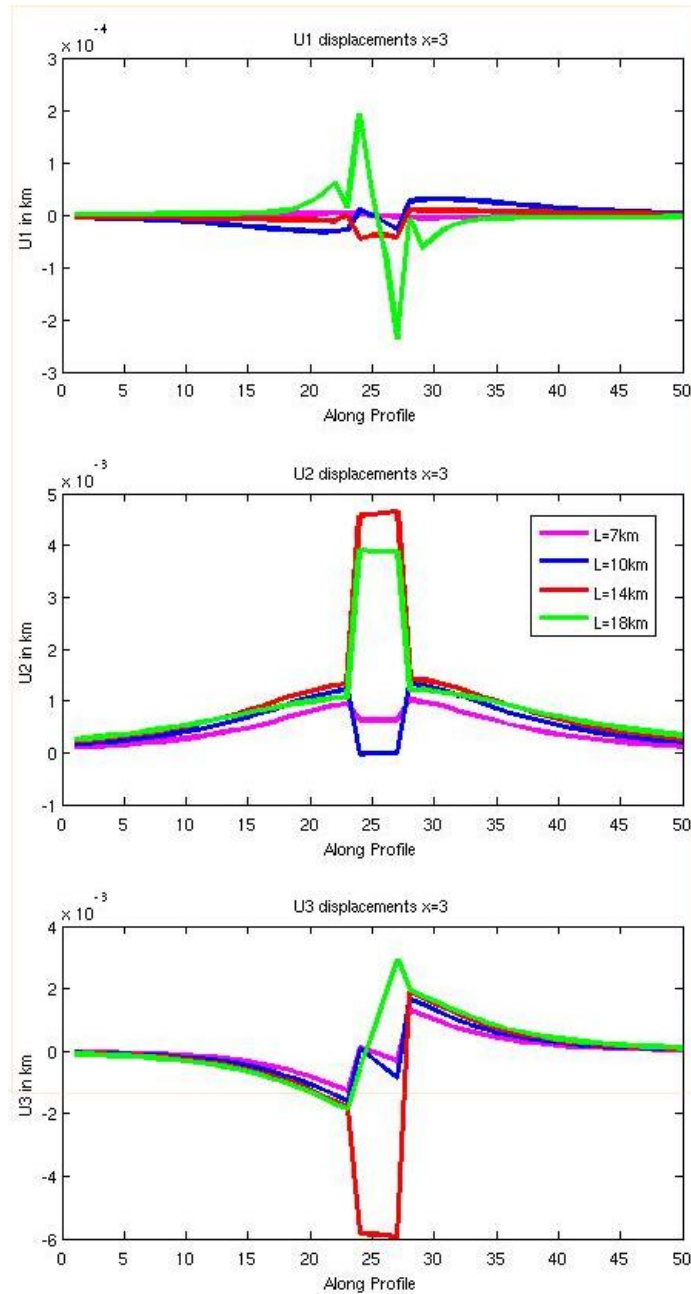


Figure 11d: As the length increased, the displacement to length ratio decreased slightly indicating that the faults are probably restricted by a mechanical boundary (Polit et al, 2005). However, if a segmented echelon geometry exists (Goudy & Schultz, 2005), lower than expected ratios may be measured. The figure shows an erratic solution for horizontal and vertical displacements (u1,u2,u3) with increasing length – across graben profiles plotted.

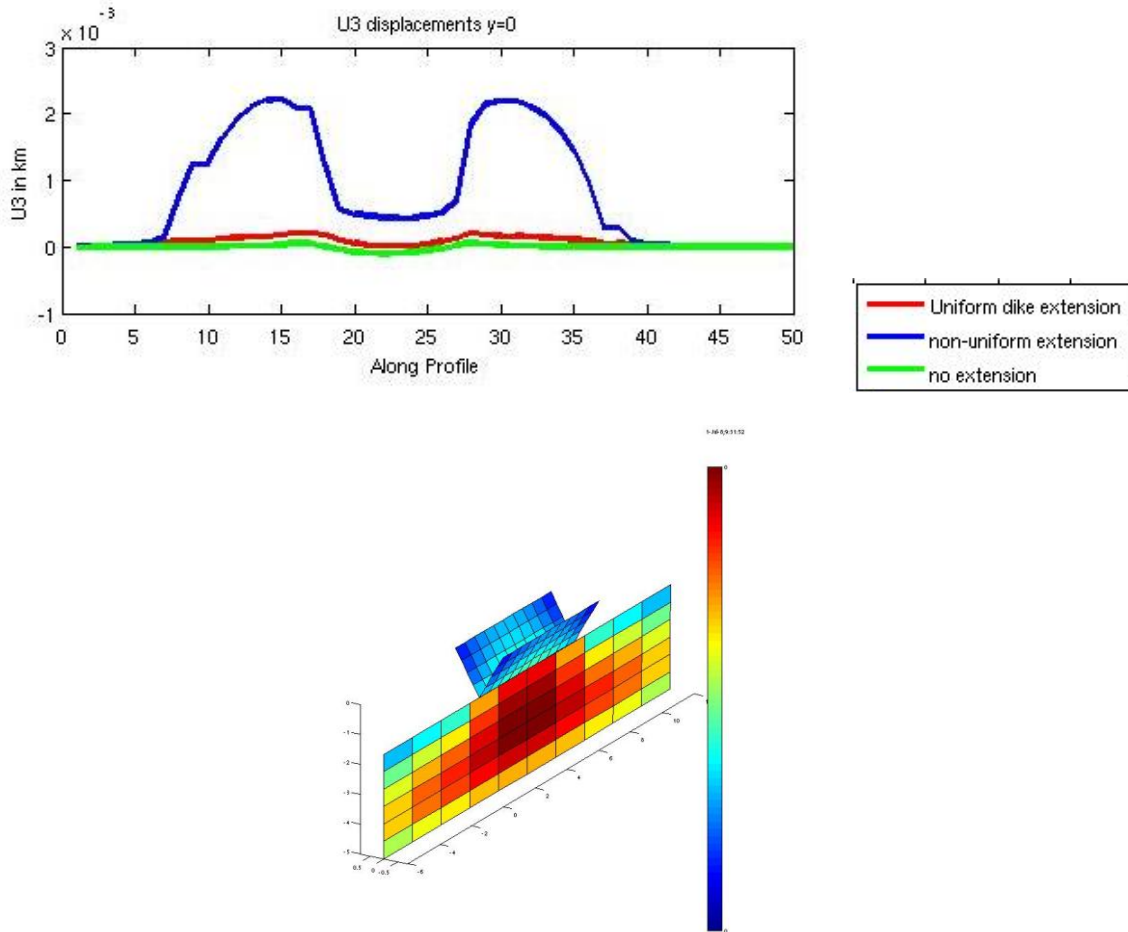


Figure 11e: A cross-graben profile of the vertical displacements is shown (top) for a dike that extends horizontally below the normal faults (bottom). More the extension, more the height of the shoulders of the graben. Non-uniform extension, i.e. the upwelling of the magma around the normal faults leads to very high shoulders. Since this is not observed in the data, this model was rejected.

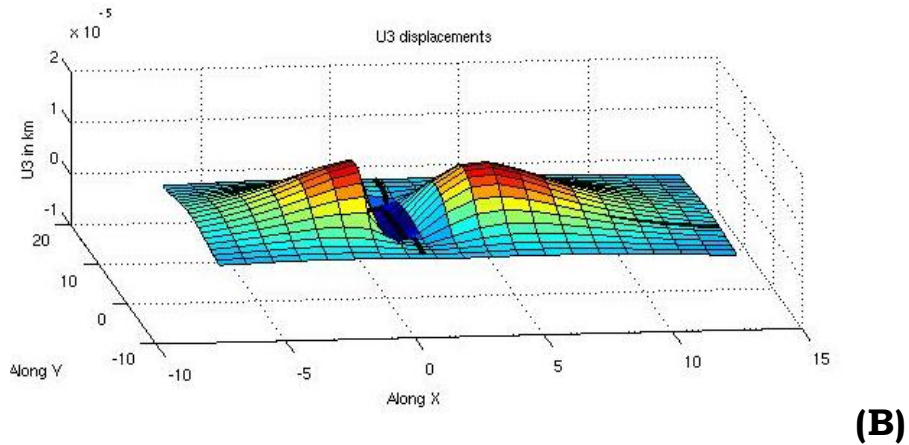
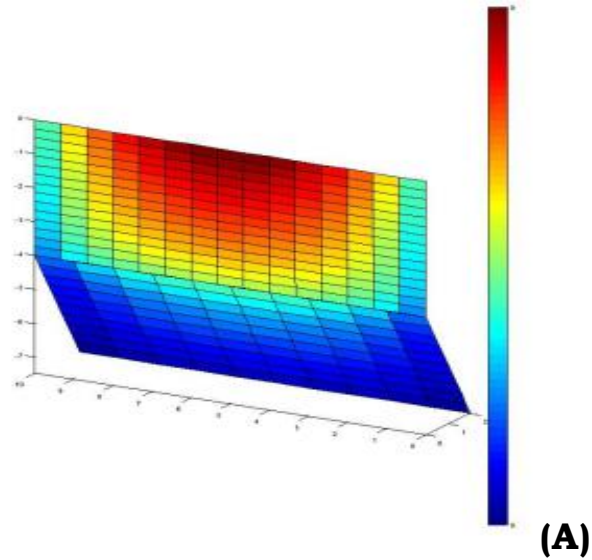


Figure 11f: (A) is a model of a normal fault at depth, which when activated causes the plane above it to open up horizontally. Thus, a graben may form even in the absence of a dike. The vertical plane is forced to have a tensile opening and zero stress on the fault. (B) shows the vertical displacement solution over the 2D grid. There is an expected asymmetry across the graben, which is not desired. Modeling experiments show that as dip of faults increases, the displacement decreases. Also, the deeper the normal fault, more the displacement due to more opening.

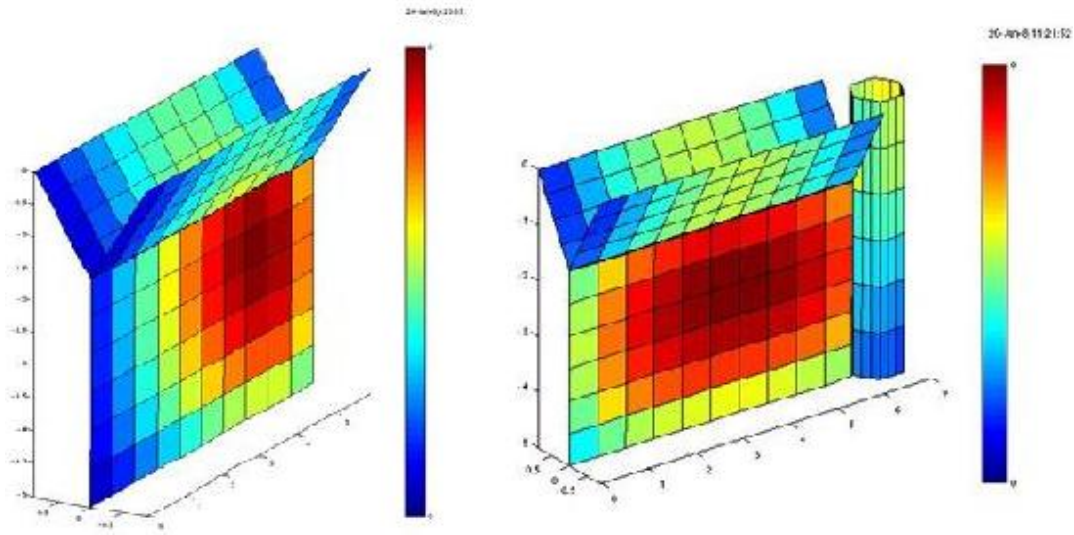
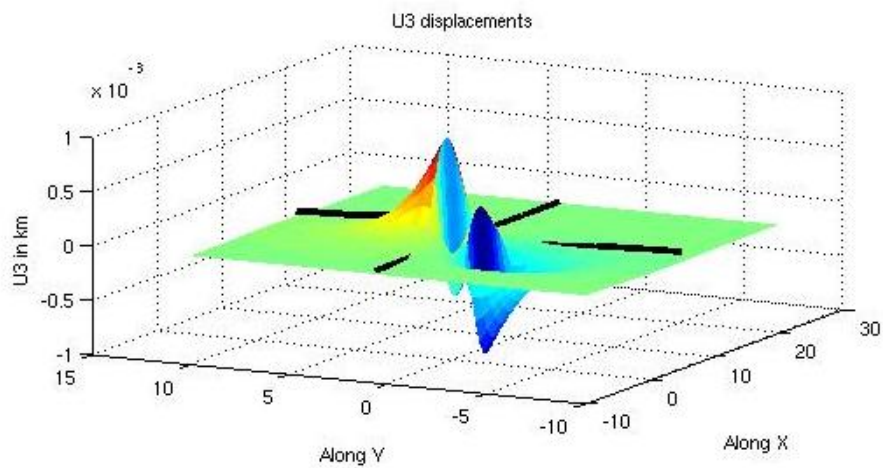
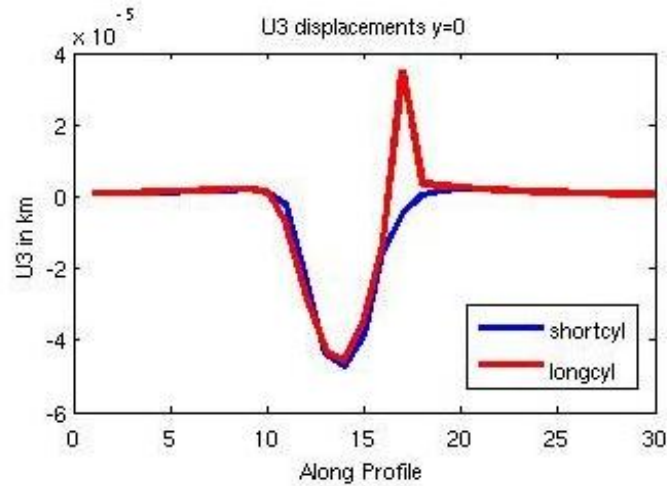


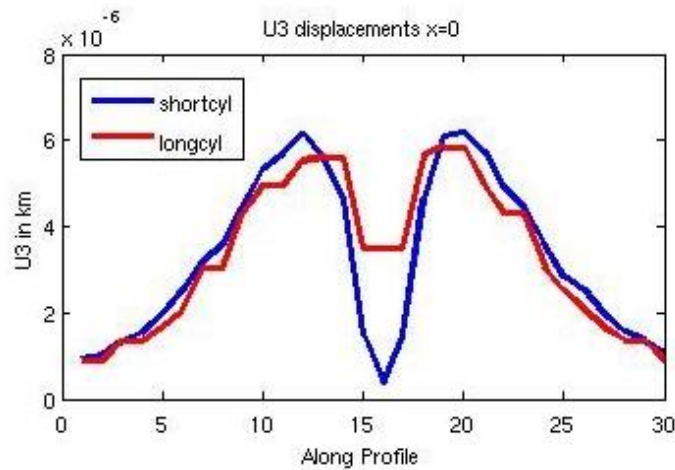
Figure 12: The model on the left forces a tensile opening on the dike increasing linearly from left to right while the boundary tractions on the normal faults is yet zero. The introduction of the cylindrical magma chamber to the right brings about the same stress conditions in the dike more realistically. The displacement solutions using these models is thus, very similar.



**(A)**



(B)



(C)

Figure 13a: (A) shows the vertical displacement from the model in 11f over the 2D observation grid. The cross and along graben profiles are also marked. (B) shows an along graben profile for a model where the cylinder reaches the surface (long cyl) and one where it terminates at the dike depth (short cyl). The magma upwelling causes an unrealistic surge of  $u_3$ . (C) shows the across graben profile.

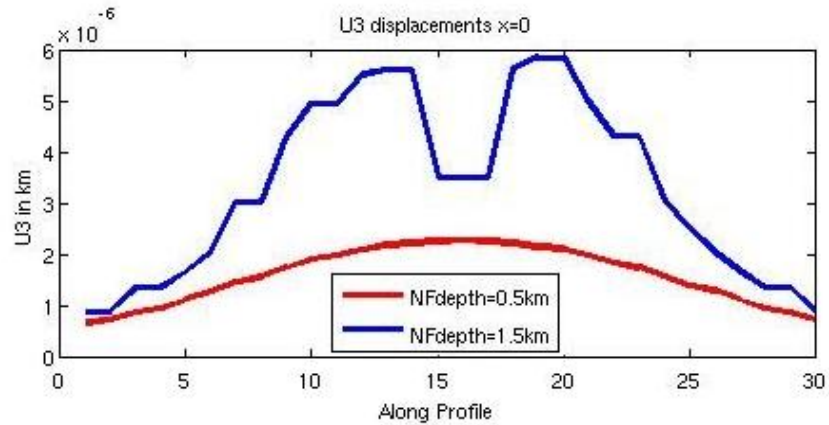
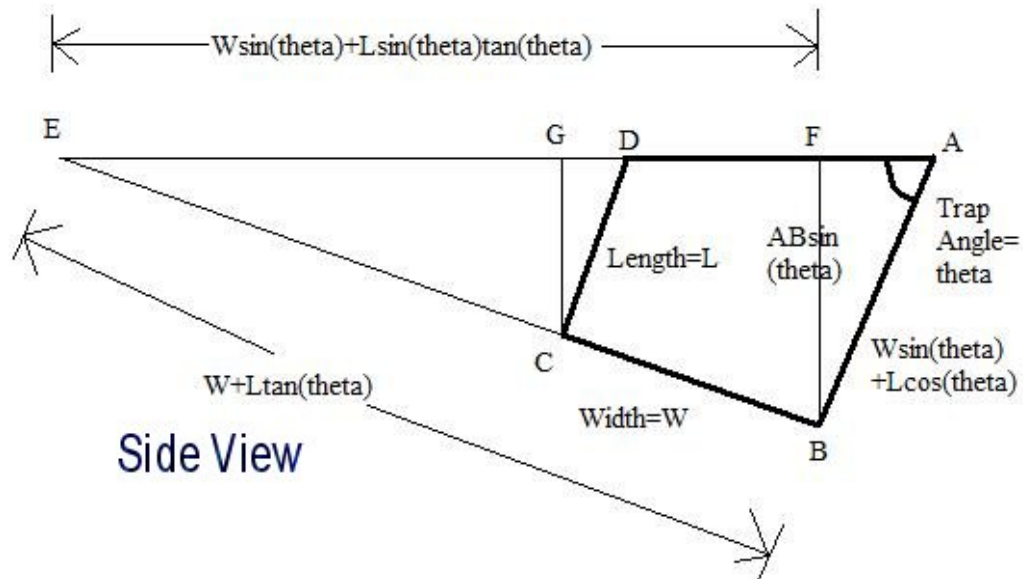


Figure 13b: This shows the effect of the width of normal fault to dike ratio. A very low ratio of 1:10 (NFDepth=0.5km, dike=5km) does not form a graben at all and gives unrealistic upthrow along strike. A moderate ratio is 1:3 (NFDepth=1.5km, dike=5km). Similarly, normal faults extending over the cylinder cause the stress distribution to move away from the dike and thus give oscillatory displacements.



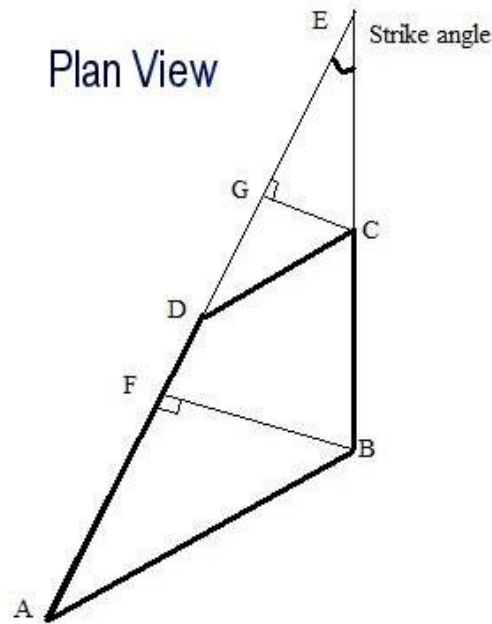


Figure 14: The dark edged polygon ABCDA represents each trapezium modeling the normal faults. Out of the 4 angles (theta, dip, strike, plunge – refer text), only 2 are independent so as to make the 2 trapeziums touch each other to form a graben with the plunging edge CB and edge DA at the Martian surface. The dike intrusion touches the base of the graben, CB.

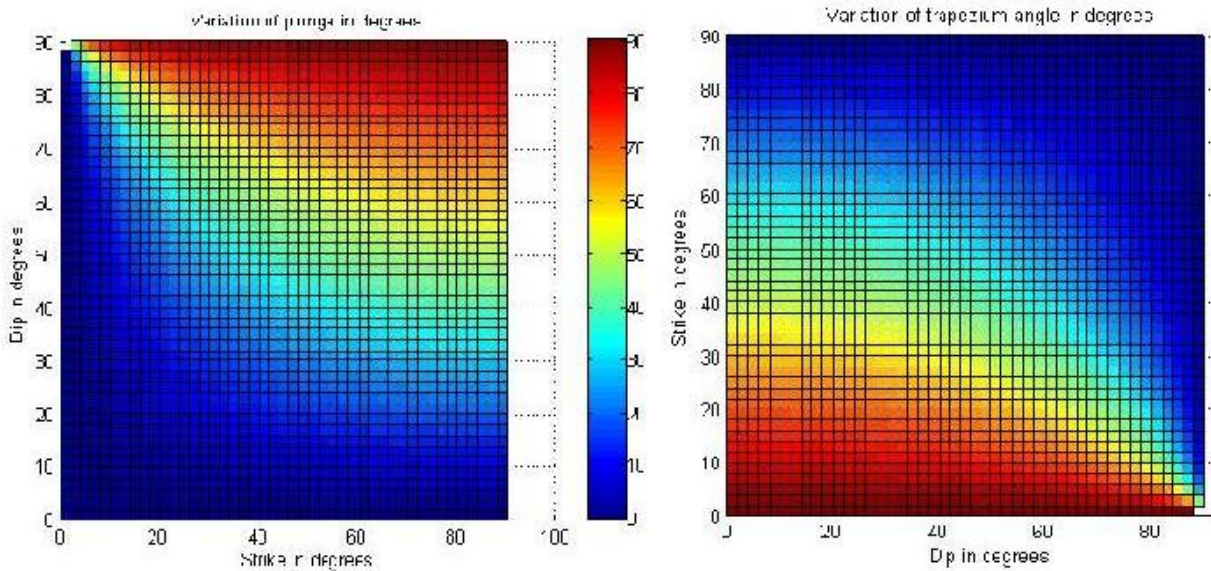
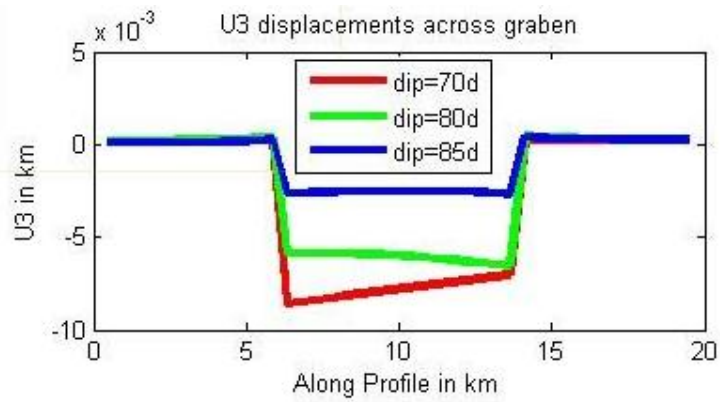
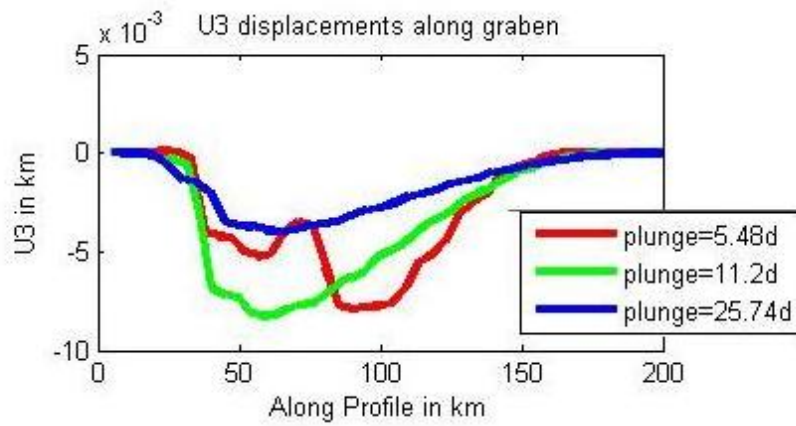


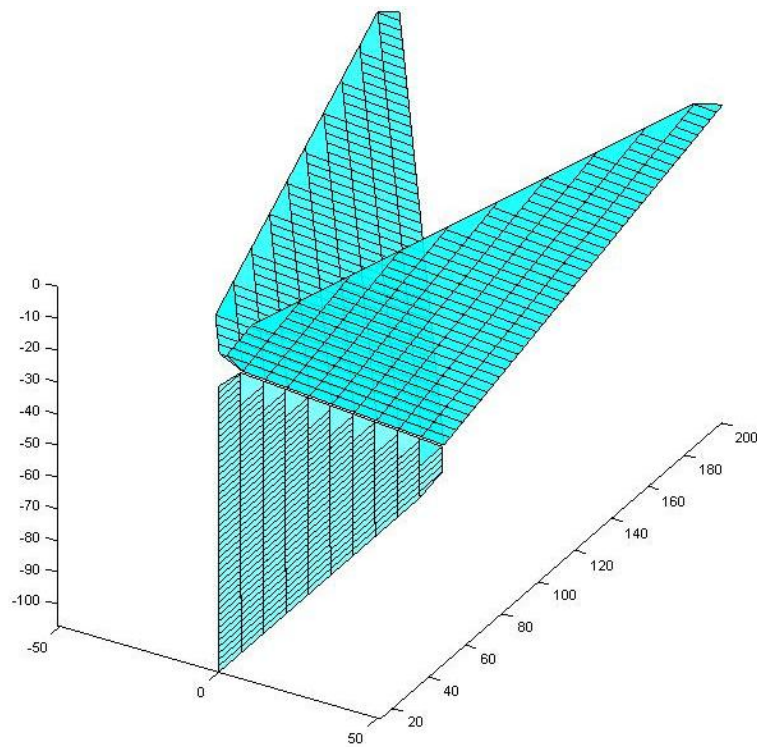
Figure 15: The angular dependence of two dependent parameters  $\theta$  and  $P$  on dip =  $\psi$  and strike =  $\phi$ . The independent parameters can be chosen per convenience.



**(A)**



**(B)**



**(C)**

Figure 16: (A) shows that increase in model dip decreases the steepness of the solution graben. The profile is a cross-graben profile where  $h=5\text{km}$ , strike=2 degrees and dip is forced to vary as specified, all other parameters calculated. The model width at this point is about 8 km too, proving that the strike does not change much from model to solution. (B) shows an along graben profile where  $h=5\text{km}$ , strike=2 degrees and plunge is forced to vary as specified, all other parameters calculated. Solution plunge reduces tremendously compared to model plunge. (C) is a test model with very low  $\theta$ , which is unnaturally skewed and gives solutions filled with artifacts.

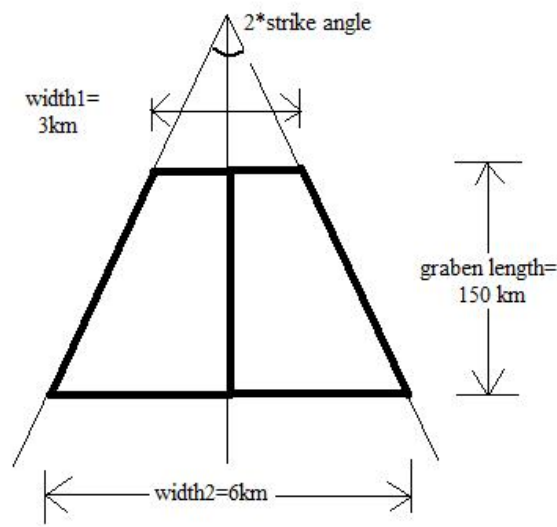


Figure 17: Calculation of the model strike angle based on the width and length of the graben from the MOLA data. Strike is less than 1 degree.

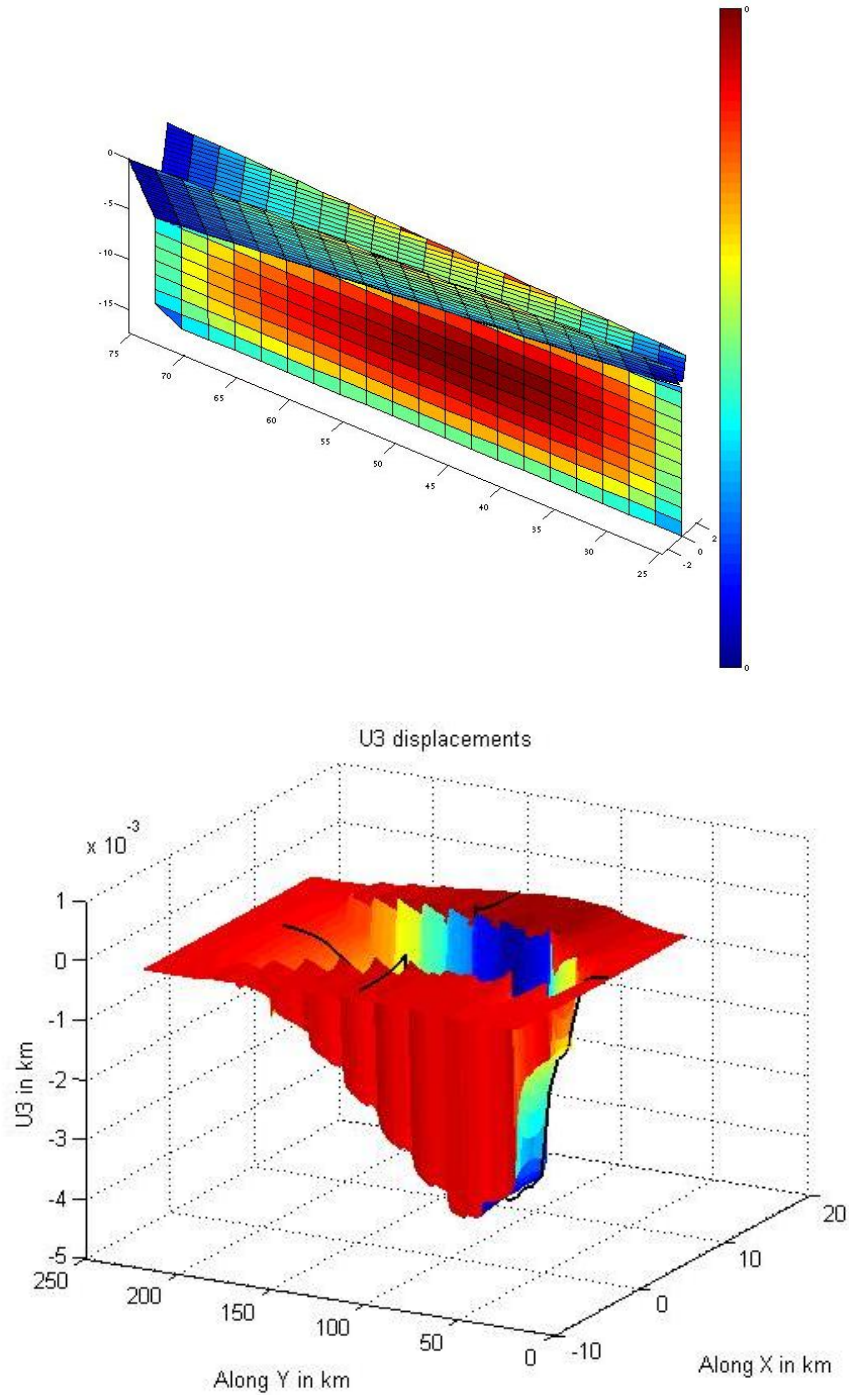


Figure 18: The final model (scaled down in distance) and vertical displacement solution as a function of the 2D observational grid. As expected, an along-strike asymmetry is seen while maintaining graben formation. As the faults in the model (above) widen and deepen, the graben in the solution widens and shallows out due to the dike going further away from the surface. The horizontal length of the model and solution are similar  $\sim 150\text{km}$ .

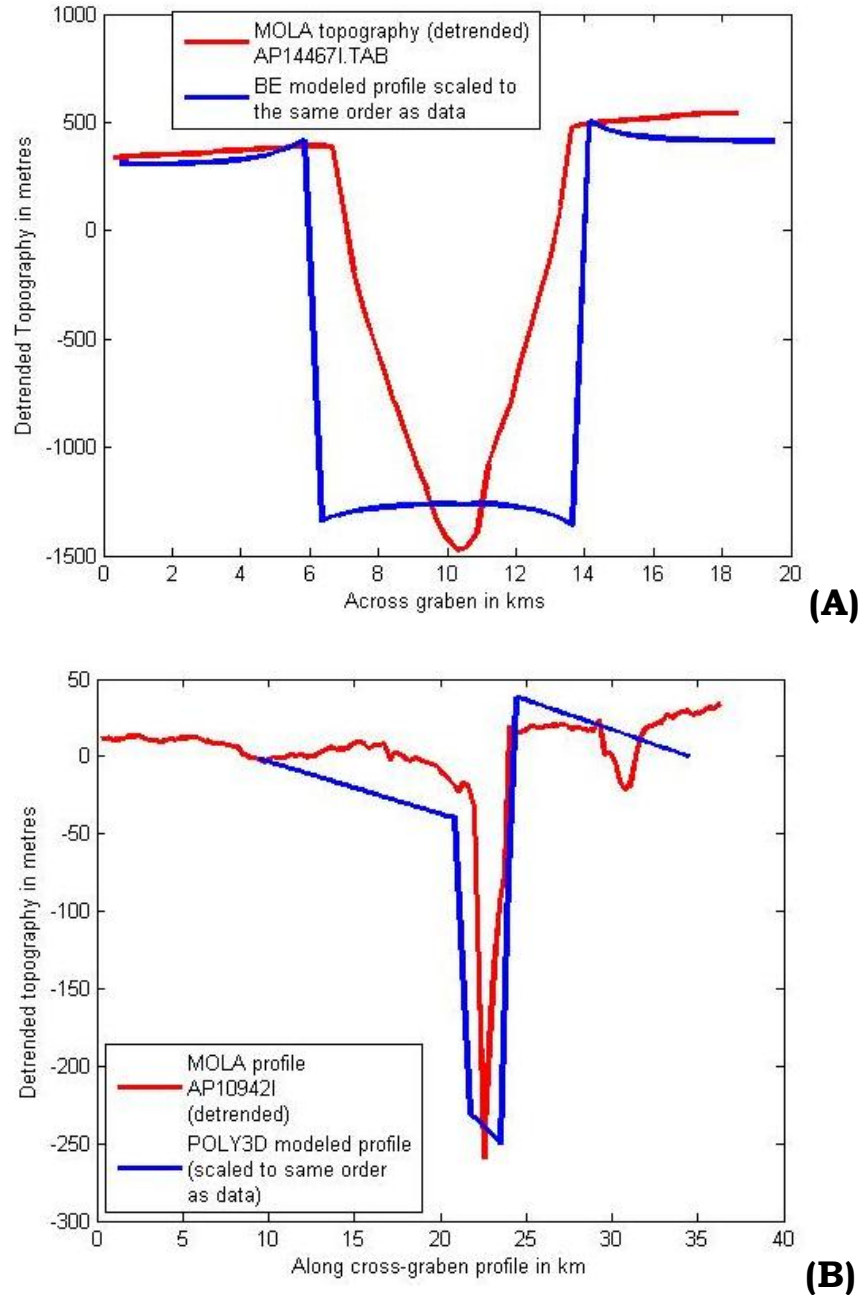


Figure 19: (A) is the comparison of a cross-graben profile of Martian topography data and the plunging model vertical displacement solution. The dike is almost 90 degrees hence the profile is symmetrical. (B) Cross-graben asymmetry is brought about by modeling the dike dipping at 75 degrees. The cross-strike asymmetry varying along the graben, implies a varying dike dip and offset.

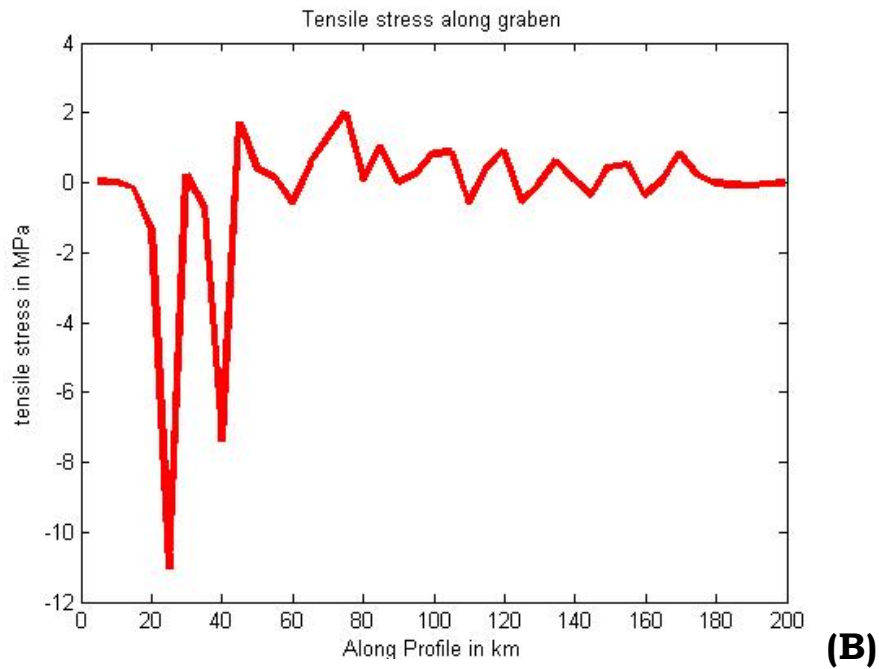
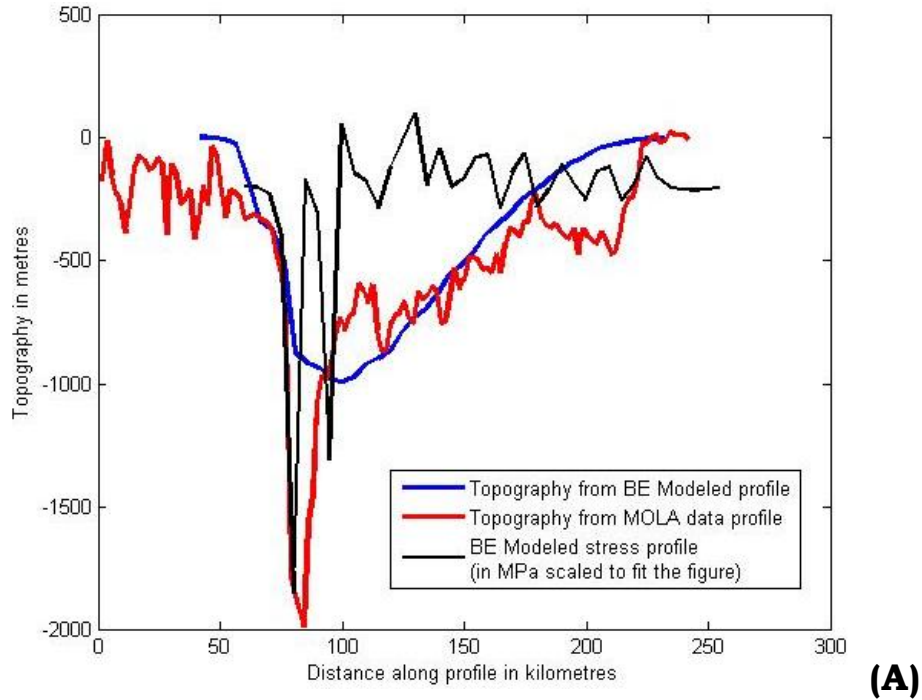


Figure 20: (A) is the comparison of a along-graben profile of Martian topography data and the plunging model vertical displacement solution. The model plunges from left to right as shown in Figure 18. The plunging model explains the deepening graben while the principal stress (shown separately in (B)) calculated along the same profile

shows a large increase at the deepest part. This extensive stress could be the cause of the pit crater/hole formation.

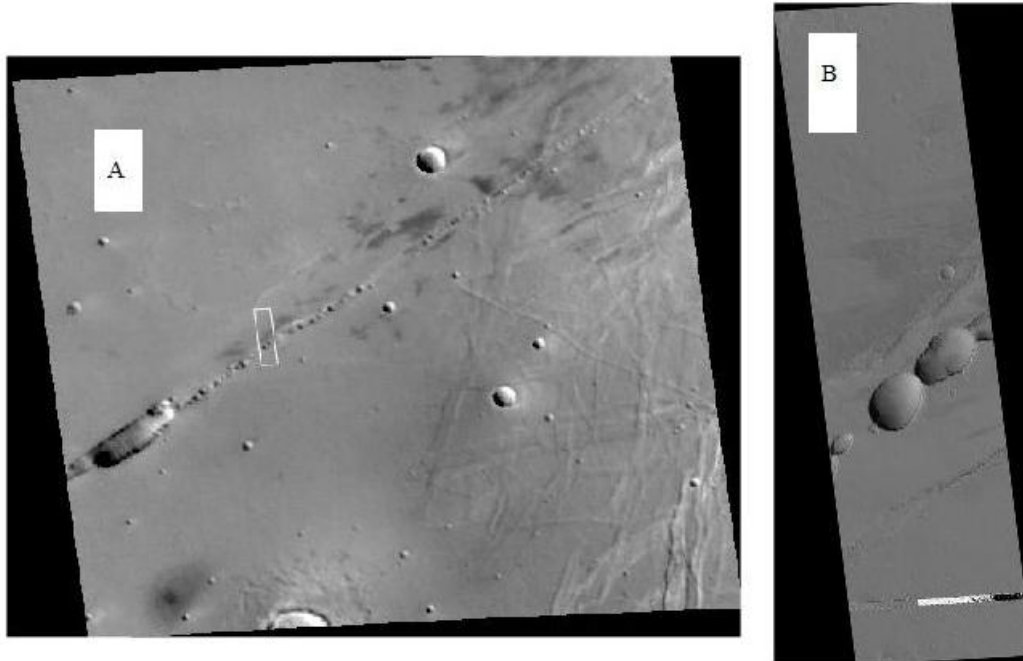


Figure 21: (A) is a wide-angle MOC image, R0501983, of the area east of the graben-and-crater system being studied, showing the presence of nothing but pit craters continuing in the strike direction. (B) Is the narrow angle view of the same, MOC narrow-angle image R0501982.

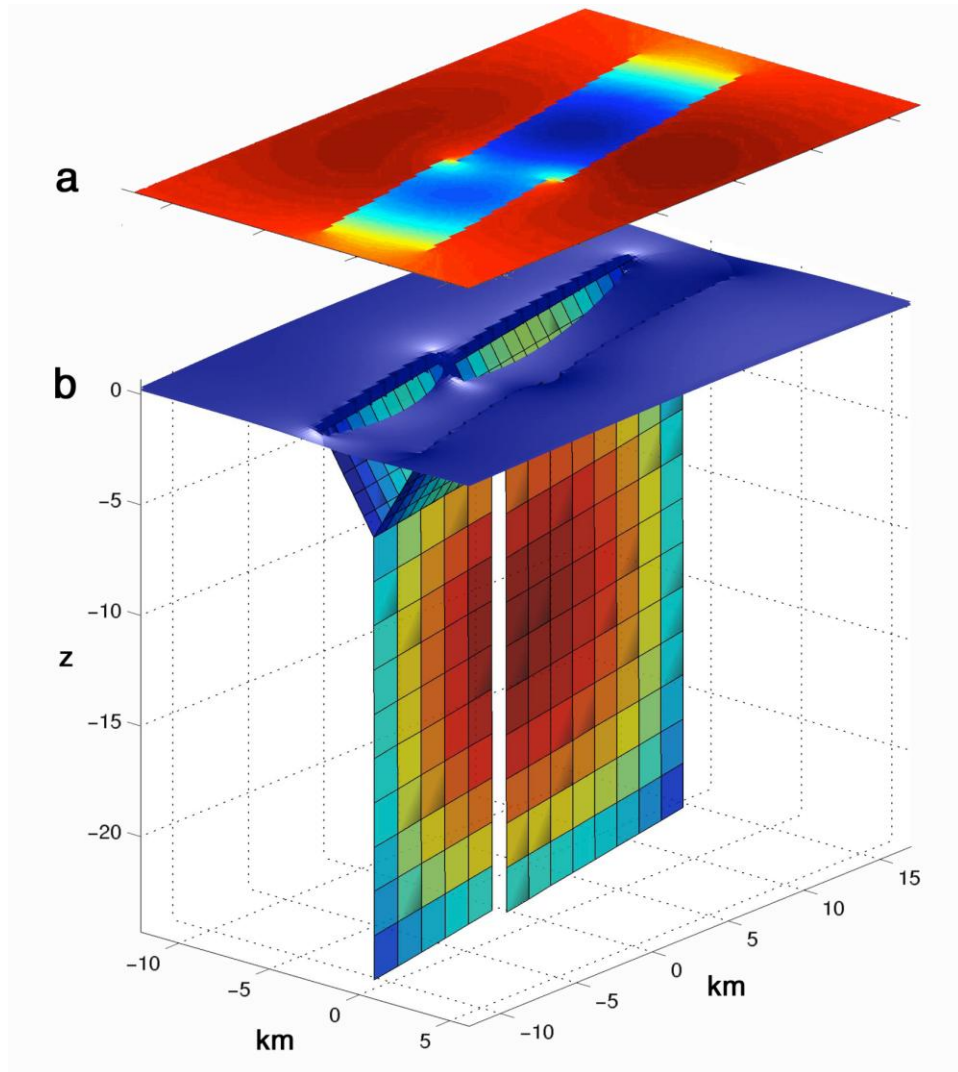


Figure 22: Example of a Poly3D solution for a dike-graben pair with small offsets between the two graben and dikes. The nearer dike is 10 km long, and the far dike is 15 km long. A unit pressure opens each dike with no ambient (external) stress field. The faults dip at  $60^\circ$ , are free of shear tractions, and remain in contact. (a) Vertical surface displacements. (blue, negative; red positive displacement). (b) Crack relative displacement magnitudes (blue, minimum amount, to red, the maximum amount; for the dikes this is mostly opening, and for the graben mostly downdip slip). The horizontal surface depicts vertically exaggerated ground displacements. The fault planes in (b) that dip towards the viewer are revealed, but those that dip away from the viewer are largely concealed by the ground surface in this perspective.